

Crystalline-Electric-Field Effect on the Resistivity of Ce-based Heavy Fermion Systems

Yasutaka NISHIDA*, Atsushi TSURUTA and Kazumasa MIYAKE

*Department of Materials Engineering Science,
Graduate School of Engineering Science, Osaka University,
Toyonaka, Osaka 560-8531*

(Received July 11, 2021)

The behavior of the resistivity of Ce-based heavy fermion systems is studied using a $1/N$ -expansion method *à la* Nagoya, where N is the spin-orbital degeneracy of f-electrons. The $1/N$ -expansion is performed in terms of the auxiliary particles, and a strict requirement of the local constraints is fulfilled for each order of $1/N$. The physical quantities can be calculated over the entire temperature range by solving the coupled Dyson equations for the Green functions self-consistently at each temperature. This $1/N$ -expansion method is known to provide asymptotically exact results for the behavior of physical quantities in both low- and high-energy regions when it is applied to a single orbital periodic Anderson model (PAM). On the basis of a generalized PAM including crystalline-electric-field splitting with a single conduction band, the pressure dependence of the resistivity ρ is calculated by parameterizing the effect of pressure as the variation of the hybridization parameter between the conduction electrons and f-electrons. The main result of the present study is that the double-peak structure of the T -dependence of $\rho(T)$ is shown to merge into a single-peak structure with increasing pressure.

KEYWORDS: Ce-based heavy fermions, electrical resistivity, $1/N$ -expansion method, crystalline electric field

1. Introduction

The resistivity of heavy fermions such as Ce-based compounds (Kondo-lattice systems) changes markedly with decreasing temperature. In the high-temperature region the conduction electrons are decoupled from the f-electrons, which behave as localized moments, exhibiting the Kondo effect that results in the logarithmic temperature dependence of the resistivity. On the other hand, below the characteristic temperature E_0 (corresponding to the Kondo temperature in an impurity model) conduction electrons are scattered coherently by the f-electrons, and a Fermi-liquid state with quasi-particles of increased mass is formed. The detailed T dependence of the resistivity $\rho(T)$ around $T = E_0$ can be roughly classified into two cases. In the first case, $\rho(T)$ has a single-peak structure as observed in CeCu₆.¹⁾ In the second case, $\rho(T)$ has a double-

*E-mail address: y-nishida@blade.mp.es.osaka-u.ac.jp

peak structure arising from the crystalline-electric-field (CEF) effect, as observed in CeAl₂,²⁾ CeCu₂,³⁾ CeAu₂Si₂,⁴⁾ CeCu₂Si₂,⁵⁾ and CeCu₂Ge₂,⁶⁾ for example. Experimental studies of the effect of pressure on Ce-based compounds have revealed the fact that the double peak in the resistivity curve arising from the CEF effect tends to merge into a single peak as the pressure is increased. In the 1980's the effect of CEF on the impurity Kondo effect was investigated theoretically by various methods.^{7,8,20,21)} However, to our knowledge, the effect of CEF in heavy fermions (lattice systems) has not been adequately investigated to date. In this work, we study the influence of the CEF effect on the T -dependence of ρ of Ce-based heavy fermions, and clarify the origin of the double-peak structure of $\rho(T)$.

To this end, we investigate an infinite- U generalized periodic Anderson model (PAM), including the CEF splitting of f-electrons, by using a $1/N$ -expansion method *à la* Nagoya, where N is the spin-orbital degeneracy of correlated electrons.^{9,10)} This $1/N$ -expansion method is performed in terms of the auxiliary particles together with strict requirement of the local constraints in each order of $1/N$ so as to rigorously take into account the effects of the infiniteness of U . As a result, the theory is free from an artificial transition of slave-boson condensation and gives correct behaviors of physical quantities in both low- and high-energy regions. Applying this method, we discuss the pressure effect of $\rho(T)$, and show that the result is consistent with the tendency observed in Ce-based heavy fermion systems.

The paper is organized as follows. In §2, we introduce the model Hamiltonian, a generalized PAM, and the concept of the $1/N$ -expansion method *à la* Nagoya. In §3, we show the result at $T = 0$ (the case of absolute zero temperature). In §4, we show results at a finite temperature by using a self-consistent $1/N$ -expansion beyond the low-temperature approximation. Finally, we show the effect of pressure on the resistivity $\rho(T)$ in §5. Three appendices are given detailing the calculation and algorithm of the $1/N$ -expansion method.

2. Model and Formal Preliminaries

2.1 Infinite- U generalized periodic Anderson model

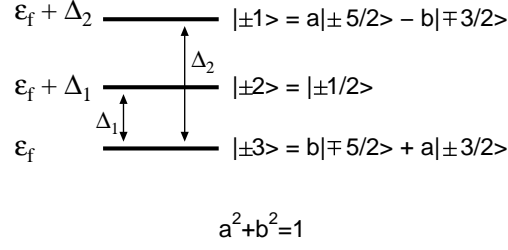
We start with an infinite- U periodic Anderson model (PAM) with an f-electron in a manifold of $J = 5/2$,¹¹⁾ which is a simple and realistic model for the Ce-based heavy fermion systems: Our model Hamiltonian is given by

$$H = H_c + H_f + H_{cf}, \quad (2.1)$$

$$H_c = \sum_{\mathbf{k}\sigma} \varepsilon_{\mathbf{k}\sigma} c_{\mathbf{k}\sigma}^\dagger c_{\mathbf{k}\sigma}, \quad (2.2)$$

$$H_f = \sum_{i\Gamma} E_{i\Gamma} f_{i\Gamma}^\dagger f_{i\Gamma}, \quad (2.3)$$

$$H_{cf} = \frac{1}{\sqrt{N_L}} \sum_{\mathbf{k}, i, \Gamma, \sigma} (V_{\mathbf{k}\Gamma\sigma} e^{-i\mathbf{k}\cdot\mathbf{R}_i} c_{\mathbf{k}\sigma}^\dagger f_{i\Gamma} b_i^\dagger + \text{h.c.}), \quad (2.4)$$

Fig. 1. CEF level scheme of Ce^{3+} ion in tetragonal symmetry.

where $c_{\mathbf{k}\sigma}^\dagger$ is the creation operator for the conduction electron with wave vector \mathbf{k} and spin σ , and $\varepsilon_{\mathbf{k}\sigma}$ is the energy of the conduction electron with wave vector \mathbf{k} and spin σ . N_L denotes the number of the lattice sites, and i stands for the site index. Here, we introduce the slave-boson, which represents the f^0 -state at each lattice point, following Coleman:¹²⁾ b_i^\dagger is the creation operator for the slave-boson at the i -th site. $f_{i\Gamma}^\dagger$ is the creation operator for the pseudo-fermion which represents the f^1 -state with the CEF level $|\Gamma\rangle = |\pm 1\rangle, |\pm 2\rangle, |\pm 3\rangle$. $V_{\mathbf{k}\Gamma\sigma}$ stands for the mixing between the conduction electron with \mathbf{k} , σ and the f-electron with the CEF state of Γ . We discuss the property of the generalized PAM introduced above assuming under a tetragonal symmetry of the crystal field. Following Kontani *et al.*,¹³⁾ the mixing $V_{\mathbf{k}\Gamma\sigma}$ is expressed as

$$V_{\mathbf{k}\Gamma\sigma} = \sum_M O_{\Gamma M} V_{\mathbf{k}M\sigma}, \quad (2.5)$$

$$V_{\mathbf{k}M\sigma} = V_0 \sqrt{\frac{4\pi}{3}} \left\{ -2\sigma \sqrt{\frac{(\frac{7}{2} - 2M\sigma)}{7}} Y_{l=3}^{M-\sigma}(\Omega_{\mathbf{k}}) \right\}, \quad (2.6)$$

where M is the z-component of the angular momentum J of an f-electron: $M = J_z$ ($J = 5/2$), and $Y_l^m(\Omega_k)$ is the spherical harmonic function. In the tetragonal symmetry, we can parameterize each CEF-level as follows: (See Fig. 1.)

$$E_{i|\pm 1\rangle} = \varepsilon_f + \Delta_2, \quad E_{i|\pm 2\rangle} = \varepsilon_f + \Delta_1, \quad E_{i|\pm 3\rangle} = \varepsilon_f. \quad (2.7)$$

ε_f is measured from the chemical potential $\varepsilon_f \equiv \varepsilon_f^{(0)} - \mu$ and $\varepsilon_f^{(0)}$ is defined as the lowest atomic level of f-electrons measured from the center of the conduction electron band. The coefficient $O_{\Gamma M}$ in eq. (2.5) is a 6×6 orthogonal matrix, which is given as follows:

$$O_{\Gamma M} = \begin{pmatrix} \Gamma \setminus M & 5/2 & 3/2 & 1/2 & -1/2 & -3/2 & -5/2 \\ +3 & 0 & a & 0 & 0 & 0 & \sqrt{1-a^2} \\ +2 & 0 & 0 & 1 & 0 & 0 & 0 \\ +1 & a & 0 & 0 & 0 & -\sqrt{1-a^2} & 0 \\ -1 & 0 & -\sqrt{1-a^2} & 0 & 0 & 0 & a \\ -2 & 0 & 0 & 0 & 1 & 0 & 0 \\ -3 & \sqrt{1-a^2} & 0 & 0 & 0 & a & 0 \end{pmatrix}. \quad (2.8)$$

$$\begin{aligned}
\mathbf{G}_{\mathbf{k}\sigma}^0 &: \text{---} \xrightarrow{\mathbf{k}_\sigma} \text{---} \\
B_i^0 &: \text{---} \overset{i}{\sim} \text{---} \\
F_{i\Gamma}^0 &: \text{---} \xrightarrow{i\Gamma} \text{---}
\end{aligned}$$

Fig. 2. Feynman diagrams: A solid line denotes the conduction electron propagator, a wavy line the slave-boson propagator, and a dashed line the pseudo-fermion propagator.

Hereafter, all the energies are measured from the chemical potential $\mu \equiv 0$.

Next, we recapitulate the $1/N$ -expansion method *à la* Nagoya. It is straightforward to extend the work by Ōno *et al.* for a single-band PAM as detailed in ref. 10. In order to ensure equivalence between the present model Hamiltonian eqs. (2.1)~(2.4) and the original infinite- U generalized PAM, we must treat the problem under the local constraints as

$$\hat{Q}_i = b_i^\dagger b_i + \sum_{\Gamma} f_{i\Gamma}^\dagger f_{i\Gamma} = 1. \quad (2.9)$$

The expectation value of an operator \hat{O} under the local constraint eq. (2.9) is given as

$$\langle \hat{O} \rangle = \lim_{\{\lambda_i\} \rightarrow \infty} \langle \hat{O} \prod_i \hat{Q}_i \rangle_\lambda / \langle \prod_i \hat{Q}_i \rangle_\lambda, \quad (2.10)$$

where $\langle \hat{A} \rangle_\lambda$ is calculated in the grand canonical ensemble for the Hamiltonian H_λ :

$$\langle \hat{A} \rangle_\lambda \equiv \text{Tr} [e^{-\beta H_\lambda} \hat{A}] / \text{Tr} [e^{-\beta H_\lambda}], \quad (2.11)$$

$$H_\lambda = H + \sum_i \lambda_i \hat{Q}_i. \quad (2.12)$$

The single-particle Green functions $G_{\mathbf{k}\sigma}$ for the conduction electron, B_i for the slave boson and $F_{i\Gamma}$ for the pseudo-fermion are essential ingredients. Their unperturbed forms are given as follows:

$$G_{\mathbf{k}\sigma}^0(i\omega_n) = (i\omega_n - \varepsilon_{\mathbf{k}\sigma})^{-1}, \quad (2.13)$$

$$B_i^0(i\nu_n) = (i\nu_n - \lambda_i)^{-1}, \quad (2.14)$$

$$F_{i\Gamma}^0(i\omega_n) = (i\omega_n - \lambda_i - E_{i\Gamma})^{-1}, \quad (2.15)$$

where $\omega_n = (2n+1)\pi T$, and $\nu_n = 2n\pi T$ with n being an integer. Then, the Feynman diagrams are illustrated in Fig. 2, and those for the *cf*-mixing vertices are illustrated in Fig. 3. The effect of the interaction, eq. (2.4), can be formally incorporated into the Green function as

self-energies as follows:

$$G_{\mathbf{k}\sigma}(i\omega_n) = (i\omega_n - \varepsilon_{\mathbf{k}\sigma} - \Sigma_{\mathbf{k}\sigma}(i\omega_n))^{-1}, \quad (2.16)$$

$$B_i(i\nu_n) = (i\nu_n - \lambda_i - \Pi_i(i\nu_n))^{-1}, \quad (2.17)$$

$$F_{i\Gamma}(i\omega_n) = (i\omega_n - E_{i\Gamma} - \lambda_i - \Sigma_{i\Gamma}^f(i\omega_n))^{-1}. \quad (2.18)$$

The self-energies $\Sigma_{\mathbf{k}\sigma}$, Π_i , and $\Sigma_{i\Gamma}^f$ are calculated by an extended $1/N$ -expansion *à la* Nagoya, as discussed below.

2.2 $1/N$ -expansion *à la* Nagoya for $SU(N)$ -PAM

We briefly review the past work performed by Ōno *et al.* as detailed in refs. 9, 10. The conventional $1/N$ -expansion method for $SU(N)$ -PAM, in which the conduction band is prepared for each component of pseudo-fermion and the hybridization depends only on \mathbf{k} , is performed by dividing the \mathbf{k} -space and spin-space of the conduction electron into N subspace and keeping the total degrees of freedom of the conduction electron to be the same as those of the non-interacting conduction band:

$$\{\uparrow, k\} + \{\downarrow, k\} = \{k_1\} + \{k_2\} + \cdots \{k_m\} + \cdots + \{k_N\}, \quad (2.19)$$

$$\sum_{m=-J}^{m=J} \left(\frac{1}{N_L} \sum_{k_m} 1 \right) = 2. \quad (2.20)$$

where N_L stands for the number of total lattice sites, $N_L \equiv \sum_i 1$. We assume that the k_m state of the conduction electron hybridizes only with the m -th state of the f-electron. Then, the density of states (DOS) of the m -th subspace of the conduction electron is $1/N$ times as small as the total DOS, so that a summation over k_m gives a factor of $1/N$. Therefore, we can classify the Feynman diagrams giving the self-energies of the Green functions in terms of $1/N$. This method may be justified on the basis of the following intuitive argument.

The state of the conduction electron with momentum \mathbf{k} and spin σ is expanded around the origin, where an f-electron is located, into that of the f-electron with the state of angular momentum state $|m\rangle$:

$$c_{\mathbf{k}\sigma} = \sum_m \sum_{k_m} \langle \sigma, \mathbf{k} | m, k_m \rangle c_{k_m}. \quad (2.21)$$

Namely, only a restricted part of the degrees of freedom \mathbf{k} and σ of the conduction electron near the Fermi level hybridizes with f-electron in the state $|m\rangle$. If the f-electron state is specified by N different quantum numbers, the degrees of freedom of conduction electrons which hybridize with the f-electron with the state $|m\rangle$ are equal to the roughly $1/N$ times of the total degrees of freedom of the conduction electron, so that the effective DOS of a relevant conduction electron is reduced by $1/N$ times. In the lattice system, hybridization between conduction electrons with \mathbf{k} and σ and the f-electron with $|m\rangle$ at the i -th site is given in

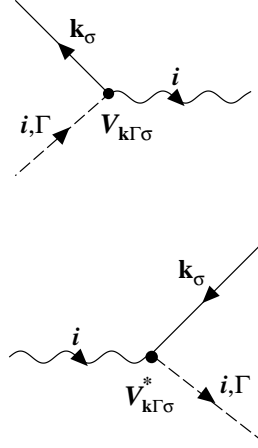


Fig. 3. Feynman diagrams for cf-hybridization: A solid line denotes the conduction electron propagator, a wavy line the slave-boson propagator, and a dashed line the pseudo-fermion propagator. These propagators are connected by the cf-hybridization vertex due to H_{cf} , eq. (2.4).

terms of the matrix element in (2.21) as

$$\langle \sigma, \mathbf{k} | k_m, m; i \rangle = e^{-i\mathbf{k} \cdot \mathbf{R}_i} \langle \sigma, \mathbf{k} | m, k_m \rangle. \quad (2.22)$$

Therefore, the Hamiltonian H_{cf} for hybridization is given as follows:

$$H_{cf} = \sum_{i,m} \sum_{\sigma, \mathbf{k}} \left(\langle \sigma, \mathbf{k} | H | m; i \rangle c_{\mathbf{k}\sigma}^\dagger f_{im} + \text{h.c.} \right), \quad (2.23)$$

$$= \sum_{i,m} \sum_{m', k_{m'}} \sum_{\sigma, \mathbf{k}} \left(\langle m', k_{m'} | \sigma, \mathbf{k} \rangle \langle \sigma, \mathbf{k} | H | m; i \rangle c_{k_{m'}}^\dagger f_{im} + \text{h.c.} \right), \quad (2.24)$$

$$= \sum_{i,m} \sum_{m', k_{m'}} \left(\langle m', k_{m'} | H | m; i \rangle c_{k_{m'}}^\dagger f_{im} + \text{h.c.} \right), \quad (2.25)$$

$$= \sum_{i,m} \sum_{m', k_{m'}} \left(\frac{1}{\sqrt{N_L}} V \delta_{m,m'} e^{-i\mathbf{k}_{m'} \cdot \mathbf{R}_i} c_{k_{m'}}^\dagger f_{im} + \text{h.c.} \right), \quad (2.26)$$

$$= \frac{1}{\sqrt{N_L}} \sum_{i,m} \sum_{k_m} \left(V c_{k_m}^\dagger f_{im} e^{-i\mathbf{k}_m \cdot \mathbf{R}_i} + \text{h.c.} \right). \quad (2.27)$$

Similarly, the Hamiltonian H_c for the kinetic term is given as follows:

$$H_c = \sum_{\sigma, \mathbf{k}} \sum_{\sigma', \mathbf{k}'} \langle \sigma, \mathbf{k} | H | \sigma', \mathbf{k}' \rangle c_{\mathbf{k}\sigma}^\dagger c_{\mathbf{k}'\sigma'}, \quad (2.28)$$

$$= \sum_{m, k_m} \sum_{m', k_{m'}} \sum_{\sigma, \mathbf{k}} \sum_{\sigma', \mathbf{k}'} \langle m, k_m | \sigma, \mathbf{k} \rangle \langle \sigma, \mathbf{k} | H | \sigma', \mathbf{k}' \rangle \langle \sigma', \mathbf{k}' | m', k_{m'} \rangle c_{k_m}^\dagger c_{k_{m'}}, \quad (2.29)$$

$$= \sum_{m, k_m} \sum_{m', k_{m'}} \langle m, k_m | H | m', k_{m'} \rangle c_{k_m}^\dagger c_{k_{m'}}, \quad (2.30)$$

$$= \sum_{m, k_m} \varepsilon_{k_m} c_{k_m}^\dagger c_{k_m}. \quad (2.31)$$

Here, we have replaced the matrix elements $\langle m', k_{m'} | H | m; i \rangle$ in eq. (2.25) with $V \delta_{m,m'} e^{-ik_m R_i} / \sqrt{N_L}$, and we have replaced $\langle m, k_m | H | m', k_{m'} \rangle$ in eq. (2.30) with $\varepsilon_{k_m} \delta_{m,m'} \delta_{k_m, k_{m'}}$. Then, the rareness of the DOS of the conduction electron for each channel m is inherited in the lattice system. In the lattice system, strictly speaking, the conduction electrons described by c_{k_m} 's mix with each other so that a classification in terms of the index m becomes ambiguous. So the approximation in eqs. (2.26) and (2.31) for the conduction electrons should be regarded as an approximation that neglects the hybridization of conduction electrons with different indices m . Nevertheless, this approximate treatment has been shown to provide reasonable results for numerous strongly correlated electron systems even for the case $N = 2$.¹⁴⁾

However, an extension of the conventional $SU(N)$ -PAM enabling inclusion of CEF splitting Δ causes a few problems: e.g., the pole of $B_i(\nu)$, E_0 which corresponds to the Kondo temperature T_K , results in contradiction, i.e., $\lambda + \varepsilon_f - E_0 > \lambda + \varepsilon_f$, if Δ is larger than almost twice T_K for $\Delta = 0$, i.e., without CEF splitting. In a word, the energy level of the coherent state becomes higher than that of the bare f-electron, and the $1/N$ -expansion method fails. For example, in the case where four degenerate states of the f-electron, i.e., $N = 4$, are divided into two Kramers doublets by CEF splitting Δ , the correct Kondo temperature $T_K^{(2)}$ for $N = 2$ is not obtained in the limit $\Delta \rightarrow \infty$. One of the origins of this difficulty may be that the hybridization between conduction electrons with different quantum numbers m is discarded, so that the two components of the conduction electrons are independent of each other. To resolve this problem, we reconsider a generalized PAM in which the conduction electron, specified by \mathbf{k} and σ , mixes with all the states of f-electrons specified by m .

2.3 Extended $1/N$ -expansion method for generalized PAM

We now apply the $1/N$ -expansion method to the generalized PAM introduced in §2.1. Namely, we extend a conventional $1/N$ -expansion method in such a way that the condition of eq. (2.20) is replaced by the following conditions.

$$\frac{1}{N_L} \sum_{k_\sigma} 1 = 1 = O(1/N), \quad (2.32)$$

$$\sum_{\sigma} 1 = 2 = O(N), \quad (2.33)$$

$$\frac{1}{N_L} \sum_{\sigma} \sum_{k_\sigma} 1 = 2 = O(1). \quad (2.34)$$

Then, the degeneracy N is given by just that of the real spin of the conduction electrons: i.e., $N = 2$. We use this condition hereafter in the present paper. As shown below, the rule of classification of the Feynman diagrams with respect to $1/N$ in the $SU(N)$ -PAM model can be generalized in the present model that has only spin degeneracy $N = 2$. The validity of using the $1/N$ -expansion method *à la* Nagoya in the case $N = 2$ is supported by the results

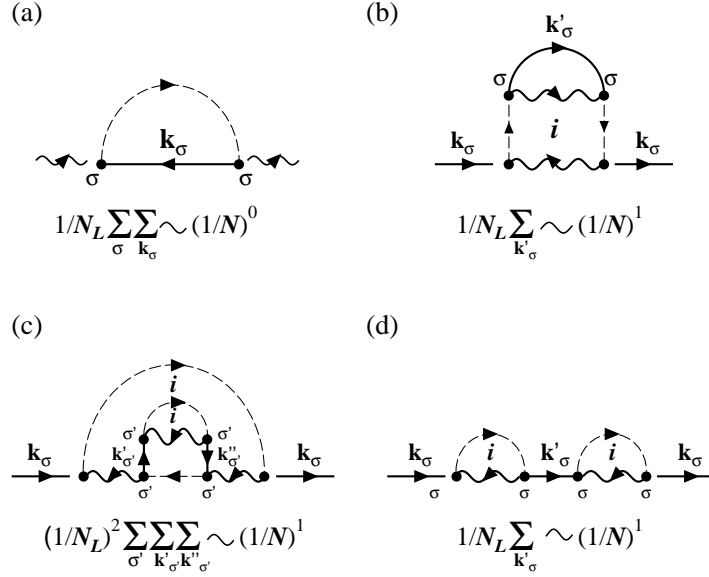


Fig. 4. Example of diagrams showing contributions to the self-energy: the lowest order of the self-energy for the slave boson (a) and the next order examples of the self-energy for the conduction electron (b,c,d) in power of $(1/N)$.

of previous studies that treated a single-band PAM with $N = 2$ and gave qualitatively correct physical behavior in both the high- and low-energy regions.¹⁴⁾ In particular, it has been shown that higher order corrections in $1/N$ do not change the results qualitatively.¹⁵⁾ On the basis of this observation, we use this $1/N$ -expansion as a method of taking into account the correlation effect of f-electrons in the present model.

The self-energies of the conduction electron $\Sigma_{\mathbf{k}\sigma}$, in eq. (2.16), the slave-boson Π_i , in eq. (2.17), and the pseudo-fermion $\Sigma_{i\Gamma}^f$, in eq. (2.18), are determined for each order of $1/N$. To classify the diagrams by each order of $(1/N)$, we use the condition in eqs. (2.32) \sim (2.34). We illustrate several examples of the self energy in Fig. 4. In our extended formulation of the $1/N$ -expansion, the diagram of Fig. 4(a) is of $O(1/N)^0$, because the summation with respect to both \mathbf{k}_σ and σ is performed as seen in eq. (2.34). On the other hand, those of Fig. 4(b), Fig. 4(c) and Fig. 4(d) are of $O(1/N)^1$ because one summation over \mathbf{k}_σ remains. For example, in Fig. 4(b), the summation $(1/N_L)^2 \sum_i \sum_{\mathbf{k}'_\sigma}$ is performed, so that this diagram gives the order of $(1/N_L) \sum_{\mathbf{k}'_\sigma} \sim O(1/N)$. Similarly, in Fig. 4(c), the summation $(1/N_L)^3 \sum_i \sum_{\sigma'} \sum_{\mathbf{k}'_{\sigma'}} \sum_{\mathbf{k}''_{\sigma'}}$ is performed. This also gives $(1/N_L)^2 \sum_{\sigma'} \sum_{\mathbf{k}'_{\sigma'}} \sum_{\mathbf{k}''_{\sigma'}} \sim (1/N_L) \sum_{\mathbf{k}''_{\sigma'}} \sim O(1/N)$. Then, for the leading order in $1/N$, the Dyson equation for the conduction electron, the slave-boson, and pseudo-fermion Green function are given by the Feynman diagrams illustrated in Fig. 5. It is noted that $\Sigma_{i\Gamma}^f$ vanishes at this order of approximation. Hereafter, we discuss the problem within the accuracy to the leading order of $1/N$, although there is no difficulty in taking into account higher order corrections in $1/N$.

$$\begin{aligned}
\mathbf{G}_{\mathbf{k}\sigma} &: \begin{array}{c} \text{Thick solid line} \\ \xrightarrow{\mathbf{k}_\sigma} \\ \sigma \quad \sigma \end{array} = \begin{array}{c} \text{Thin solid line} \\ \xrightarrow{\mathbf{k}_\sigma} \\ \sigma \quad \sigma \end{array} + \begin{array}{c} \text{Thin solid line} \\ \xrightarrow{\mathbf{k}_\sigma} \\ \sigma \quad \sigma \end{array} \left[\begin{array}{c} \text{Loop with } i \text{ and } \Gamma \\ \text{wavy line } i \\ \text{dashed line } i, \Gamma \\ \text{wavy line } i \\ \text{dashed line } i, \Gamma \end{array} \right] \begin{array}{c} \text{Thick solid line} \\ \xrightarrow{\mathbf{k}_\sigma} \\ \sigma \quad \sigma \end{array} \\
\mathbf{B}_i &: \begin{array}{c} \text{Wavy line } i \\ \text{Thin solid line} \end{array} = \begin{array}{c} \text{Wavy line } i \\ \text{Thin solid line} \end{array} + \begin{array}{c} \text{Wavy line } i \\ \text{Thin solid line} \end{array} \left[\begin{array}{c} \text{Loop with } i, \Gamma \\ \text{wavy line } i \\ \text{dashed line } i, \Gamma \\ \text{wavy line } i \\ \text{dashed line } i, \Gamma \end{array} \right] \begin{array}{c} \text{Wavy line } i \\ \text{Thin solid line} \end{array} \\
\mathbf{F}_{i\Gamma} &: \begin{array}{c} \text{Dashed line } i, \Gamma \\ \text{Thin dashed line} \end{array} = \begin{array}{c} \text{Dashed line } i, \Gamma \\ \text{Thin dashed line} \end{array}
\end{aligned}$$

Fig. 5. Diagrammatic representation of Dyson equations for single particle Green function within accuracy of $(1/N)^0$. Thin solid, wavy, and dashed lines represent the Green function of the conduction electron, slave-boson, and pseudo-fermion, respectively. Thick lines denote the renormalized Green function for each particle.

2.4 Dyson equation to the leading order in $(1/N)^0$

When treating the problem under zero magnetic field or without magnetic order, we can neglect the off-diagonal self-energy part, with respect to the spin, of the conduction electrons, because of the properties of the Clebsch-Gordan coefficient. Indeed, from the relation of spherical harmonic function $\{Y_l^m(\Omega_k)\}^* = (-1)^m Y_l^{-m}(\Omega_k)$, we can find

$$\sum_{\Gamma\pm} V_{\mathbf{k}\Gamma\sigma}^* V_{\mathbf{k}\Gamma\bar{\sigma}} = 0, \quad (2.35)$$

$$\sum_{\Gamma\pm} |V_{\mathbf{k}\Gamma\sigma}|^2 = \sum_{\Gamma\pm} |V_{\mathbf{k}\Gamma\bar{\sigma}}|^2, \quad (2.36)$$

where $\bar{\sigma} = -\sigma$ and $\sum_{\Gamma\pm}$ means the summation with respect to the Kramers doublets characterized with $|\Gamma\rangle = |\pm 1\rangle, |\pm 2\rangle, \text{ and } |\pm 3\rangle$. For $\Gamma = |\pm 1\rangle$, eq. (2.35) means that $V_{\mathbf{k}|+1\sigma}^* V_{\mathbf{k}|+1\bar{\sigma}} + V_{\mathbf{k}|-1\sigma}^* V_{\mathbf{k}|-1\bar{\sigma}} = 0$ is satisfied. The analytic form of the relevant self-energy parts are given by

$$\Sigma_{\mathbf{k}\sigma}(i\omega_n) = \lim_{\lambda_i \rightarrow \infty} \left[- \sum_{\Gamma\pm} |V_{\mathbf{k}\Gamma\sigma}|^2 T \sum_{\nu_n} B_i(i\nu_n) F_{i\Gamma}^0(i\omega_n + i\nu_n) / \langle \hat{Q}_i \rangle_\lambda \right], \quad (2.37)$$

$$\Pi_i(i\nu_n) = \frac{1}{N_L} \sum_{\Gamma\pm} \sum_{\sigma} \sum_{\mathbf{k}\sigma} |V_{\mathbf{k}\Gamma\sigma}|^2 T \sum_{\omega_n} G_{\mathbf{k}\sigma}(i\omega_n) F_{i\Gamma}^0(i\omega_n + i\nu_n), \quad (2.38)$$

$$\langle \hat{Q}_i \rangle_\lambda = \sum_{\Gamma\pm} \langle \hat{n}_{fi\Gamma} \rangle_\lambda + \langle \hat{n}_{bi} \rangle_\lambda. \quad (2.39)$$

Here, $\langle \hat{n}_{fi\Gamma} \rangle_\lambda \equiv \langle f_{i\Gamma}^\dagger f_{i\Gamma} \rangle_\lambda$ and $\langle \hat{n}_{bi} \rangle_\lambda \equiv \langle b_i^\dagger b_i \rangle_\lambda$ are given by the diagrams shown in Fig. 6 whose analytic forms are given as follows:

$$\langle \hat{n}_{fi\Gamma} \rangle_\lambda = T \sum_{\omega_n} F_{i\Gamma}^0(i\omega_n) \quad (2.40)$$

$$- \frac{1}{N_L} \sum_{\sigma} \sum_{\mathbf{k}\sigma} |V_{\mathbf{k}\Gamma\sigma}|^2 T^2 \sum_{\omega_n} \sum_{\nu_n} F_{i\Gamma}^0(i\omega_n + i\nu_n)^2 G_{\mathbf{k}\sigma}(i\omega_n) B_i(i\nu_n), \quad (2.41)$$

$$\langle \hat{n}_{bi} \rangle_\lambda = -T \sum_{\nu_n} B_i(i\nu_n). \quad (2.42)$$

Taking the summation with respect to the Matsubara frequency in eqs. (2.37) and (2.38), and performing the analytic continuation $i\omega_n \rightarrow \omega_+ \equiv \omega + i0_+$, we obtain the imaginary part and real part of the self-energies as follows:

$$\begin{aligned} \text{Im}\Sigma_{\mathbf{k}\sigma}(\omega_+) &= \lim_{\lambda_i \rightarrow \infty} \sum_{\Gamma_\pm} |V_{\mathbf{k}\Gamma\sigma}|^2 \left(1 + e^{\beta\omega}\right) e^{-\beta(\lambda_i + E_{i\Gamma})} \\ &\quad \times \text{Im}B_i(-\omega + \lambda_i + E_{i\Gamma} + i0_+)/\langle \hat{Q}_i \rangle_\lambda, \end{aligned} \quad (2.43)$$

$$\text{Re}\Sigma_{\mathbf{k}\sigma}(\omega_+) = -\frac{1}{\pi} P \int_{-\infty}^{\infty} d\omega' \frac{1}{\omega - \omega' + i0_+} \text{Im}\Sigma_{\mathbf{k}\sigma}(\omega'_+), \quad (2.44)$$

$$\begin{aligned} \text{Im}\Pi_i(\omega_+) &= \frac{1}{N_L} \sum_{\Gamma_\pm} \sum_{\sigma} \sum_{\mathbf{k}_\sigma} |V_{\mathbf{k}\Gamma\sigma}|^2 f(-\omega + \lambda_i + E_{i\Gamma}) \\ &\quad \times \text{Im}G_{\mathbf{k}\sigma}(-\omega + \lambda_i + E_{i\Gamma} + i0_+), \end{aligned} \quad (2.45)$$

$$\text{Re}\Pi_i(\omega_+) = -\frac{1}{\pi} P \int_{-\infty}^{\infty} d\omega' \frac{1}{\omega - \omega' + i0_+} \text{Im}\Pi_i(\omega'_+), \quad (2.46)$$

where $f(\omega) \equiv (e^{\beta\omega} + 1)^{-1}$ is the Fermi distribution function ($\beta \equiv 1/T$). The real part of the self-energies are given by the Kramers-Krönig relation from the corresponding imaginary part of the self-energy. Of course, we can calculate $\Sigma_{\mathbf{k}\sigma}$ and Π_i analytically without separating the real and imaginary parts. However, we express them in such a way for convenience of the numerical calculation.

Here, we introduce characteristic parameters E_0 and a . From eqs. (2.17), (2.45), and (2.46), we can find the following relation at low temperature ($T \lesssim E_0/10$, as shown later).

$$-\frac{1}{\pi} \text{Im}B_i(\omega_+) = a(T) \cdot \delta(\omega + \lambda_i + \varepsilon_f + E_0(T)) + C(\omega + \lambda_i + \varepsilon_f), \quad (2.47)$$

where $C(\omega + \lambda_i + \varepsilon_f)$ is a broad continuous function that is non-vanishing only in the region of $\omega > 0$, and the binding energy $E_0(T)$ and the residue $a(T)$ of the slave-boson are determined through the coupled relations

$$E_0(T) = \varepsilon_f - \text{Re}\Pi_i(\lambda_i + \varepsilon_f - E_0(T)), \quad (2.48)$$

$$\frac{1}{a} = 1 - \frac{d}{d\omega} (\text{Re}\Pi_i(\omega))|_{\omega=\lambda_i+\varepsilon_f-E_0(T)}. \quad (2.49)$$

The parameter $E_0 \equiv E_0(0)$ corresponds to the Kondo temperature T_K in the case of impurity Anderson model.¹⁶⁾ To express a series of equations more concisely in the actual numerical calculation, we introduce the following notations: $\langle \hat{Q}_i \rangle_\lambda = e^{-\beta(\lambda_i + \varepsilon_f - E_0(T))} \langle \hat{Q} \rangle$, $\bar{B}(\omega) = B_i(\omega + \lambda_i + \varepsilon_f)$ and $\bar{\Pi}(\omega) = \Pi_i(\omega + \lambda_i + \varepsilon_f)$. Then, we can rewrite eqs. (2.37)~(2.42) as follows:

$$\begin{aligned} \text{Im}\Sigma_{\mathbf{k}\sigma}(\omega_+) &= \sum_{\Gamma_\pm} |V_{\mathbf{k}\Gamma\sigma}|^2 \left(1 + e^{\beta\omega}\right) e^{-\beta[E_0(T) + E_{i\Gamma} - \varepsilon_f]} \\ &\quad \times \text{Im}\bar{B}(-\omega + E_{i\Gamma} - \varepsilon_f + i0_+)/\langle \hat{Q} \rangle, \end{aligned} \quad (2.50)$$

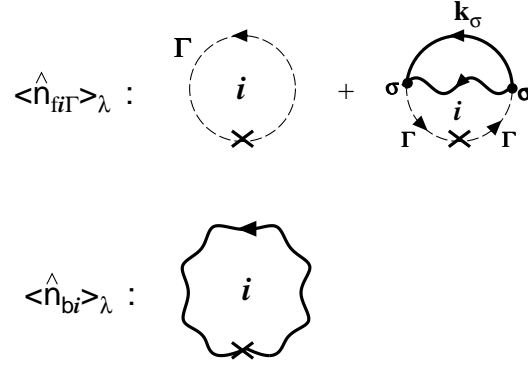


Fig. 6. Feynman diagrams for $\langle \hat{n}_{fi\Gamma} \rangle_\lambda$, and $\langle \hat{n}_{bi} \rangle_\lambda$ within the order of $(1/N)^0$.

$$\begin{aligned} \text{Im}\bar{\Pi}(\omega_+) &= \frac{1}{N_L} \sum_{\Gamma\pm} \sum_{\sigma} \sum_{\mathbf{k}_\sigma} |V_{\mathbf{k}\Gamma\sigma}|^2 f(-\omega + E_{i\Gamma} - \varepsilon_f) \\ &\quad \times \text{Im}G_{\mathbf{k}\sigma}(-\omega + E_{i\Gamma} - \varepsilon_f + i0_+), \end{aligned} \quad (2.51)$$

and

$$\begin{aligned} \langle \hat{n}_{fi\Gamma} \rangle_\lambda &= e^{-\beta(\lambda_i + \varepsilon_f - E_0(T))} \times \left[e^{-\beta[E_0(T) + E_{i\Gamma} - \varepsilon_f]} \right. \\ &\quad + \sum_{\sigma} \sum_{\mathbf{k}_\sigma} \frac{|V_{\mathbf{k}\Gamma\sigma}|^2}{N_L} \int d\omega f(\omega) \frac{-1}{\pi} \text{Im}G_{\mathbf{k}\sigma}(\omega_+) \\ &\quad \times \int d\omega' e^{-\beta(E_0(T) + \omega')} \frac{-1}{\pi} \text{Im}\bar{B}(\omega'_+) \cdot \frac{1}{(\omega + \omega' - E_{i\Gamma} + \varepsilon_f)^2} \\ &\quad + \sum_{\sigma} \sum_{\mathbf{k}_\sigma} \frac{|V_{\mathbf{k}\Gamma\sigma}|^2}{N_L} \int d\omega e^{-\beta(E_0(T) + E_{i\Gamma} - \varepsilon_f)} \frac{-1}{\pi} \text{Im}G_{\mathbf{k}\sigma}(-\omega + i0_+) \\ &\quad \left. \times f(\omega) \cdot \left\{ \frac{-1}{T} \bar{B}(\omega + E_{i\Gamma} - \varepsilon_f) + \frac{d\bar{B}(\omega')}{d\omega'} \Big|_{\omega' = \omega + E_{i\Gamma} - \varepsilon_f} \right\} \right], \end{aligned} \quad (2.52)$$

$$\langle \hat{n}_{bi} \rangle_\lambda = e^{-\beta(\lambda_i + \varepsilon_f - E_0(T))} \times \int d\omega e^{-\beta(\omega + E_0(T))} \frac{-1}{\pi} \text{Im}\bar{B}(\omega_+). \quad (2.53)$$

The validity of the approximate eq. (2.47) in the low-temperature region, or eq. (2.54) below, for \bar{B} is shown in the next subsection, while in high-temperature region ($T > E_0$) eq. (2.47) ceases to be valid.

$$-\frac{1}{\pi} \text{Im}\bar{B}(\omega_+) = a(T) \cdot \delta(\omega + E_0(T)) + C(\omega). \quad (2.54)$$

To extend this formulation to a finite temperature region, we must use the Dyson equation self-consistently (See §4).

Finally we calculate the average number n_c of conduction electrons and n_f of f-electrons per site:

$$n_c \equiv \frac{1}{N_L} \sum_{\sigma} \sum_{\mathbf{k}_\sigma} \left[T \sum_{\omega_n} G_{\mathbf{k}\sigma}(i\omega_n) e^{i\omega_n 0_+} \right], \quad (2.55)$$

$$n_f \equiv \lim_{\lambda_i \rightarrow \infty} \left[\sum_{\Gamma_{\pm}} \langle \hat{n}_{f i \Gamma} \rangle_{\lambda} / \langle \hat{Q}_i \rangle_{\lambda} \right]. \quad (2.56)$$

With the use of eqs. (2.37) and (2.41), we obtain

$$n_f = \lim_{\lambda_i \rightarrow \infty} \sum_{\Gamma_{\pm}} \left[T \sum_{\omega_n} F_{i \Gamma}^0(i\omega_n) / \langle \hat{Q}_i \rangle_{\lambda} \right] \quad (2.57)$$

$$+ \frac{1}{N_L} \sum_{\sigma} \sum_{\mathbf{k}_{\sigma}} \left[-T \sum_{\omega_n} G_{\mathbf{k}\sigma}(i\omega_n) \frac{d}{d(i\omega_n)} \Sigma_{\mathbf{k}\sigma}(i\omega_n) \right]. \quad (2.58)$$

Hence, the total number of electrons per site is given by

$$\begin{aligned} n_c + n_f &= \lim_{\lambda_i \rightarrow \infty} \sum_{\Gamma_{\pm}} \left[T \sum_{\omega_n} F_{i \Gamma}^0(i\omega_n) / \langle \hat{Q}_i \rangle_{\lambda} \right] \\ &\quad + \frac{1}{N_L} \sum_{\sigma} \sum_{\mathbf{k}_{\sigma}} \left[T \sum_{\omega_n} \frac{d}{d(i\omega_n)} \log G_{\mathbf{k}\sigma}^{-1}(i\omega_n) \right], \end{aligned} \quad (2.59)$$

$$\begin{aligned} &= \sum_{\Gamma_{\pm}} e^{-\beta(E_0(T) + E_{i \Gamma} - \varepsilon_f)} / \langle \hat{Q} \rangle \\ &\quad + \frac{1}{N_L} \sum_{\sigma} \sum_{\mathbf{k}_{\sigma}} \left[T \sum_{\omega_n} \frac{d}{d(i\omega_n)} \log G_{\mathbf{k}\sigma}^{-1}(i\omega_n) \right]. \end{aligned} \quad (2.60)$$

At $T = 0$, this relation is simplified as

$$n_c + n_f = \frac{1}{N_L} \sum_{\sigma} \sum_{\mathbf{k}_{\sigma}} \left[T \sum_{\omega_n} \frac{d}{d(i\omega_n)} \log G_{\mathbf{k}\sigma}^{-1}(i\omega_n) \right]. \quad (2.61)$$

Furthermore, we find $\text{Im} \Sigma_{\mathbf{k}\sigma}(0_+) = 0$ at $T = 0$ from eqs. (2.50) and (2.54), so that we obtain the total number $n \equiv n_c + n_f$ as

$$n = n_c + n_f = \frac{1}{N_L} \sum_{\sigma} \sum_{\mathbf{k}_{\sigma}} \theta(-\varepsilon_{\mathbf{k}\sigma} - \Sigma_{\mathbf{k}\sigma}(0)). \quad (2.62)$$

The total number is determined by the volume of the k -space enclosed by the Fermi surface. In a word, the Landau-Luttinger sum-rule holds at $T = 0$ ¹⁷⁾.

3. Physical properties of Generalized Periodic Anderson Model at $T = 0$

In this section, we study the properties of the generalized PAM (2.1)~(2.4) in the limit of $T \rightarrow 0$, where eq. (2.54) (or eq. (2.47)) is a valid approximation. (See § 3.2) With the use of eq. (2.54), we manipulate eqs. (2.52) and (2.53) as follows. From eqs. (2.52) ~ (2.54)

$$\begin{aligned} \langle \hat{n}_{f i \Gamma} \rangle_{\lambda} &= e^{-\beta(\lambda_i + \varepsilon_f - E_0)} \\ &\quad \times \left[e^{-\beta(E_0 + E_{i \Gamma} - \varepsilon_f)} \right. \\ &\quad + \sum_{\sigma} \sum_{\mathbf{k}_{\sigma}} \frac{a |V_{\mathbf{k}\Gamma\sigma}|^2}{N_L} \int d\omega \frac{-1}{\pi} \text{Im} G_{\mathbf{k}\sigma}(\omega_+) \cdot \frac{f(\omega)}{(\omega - E_0 - E_{i \Gamma} + \varepsilon_f)^2} \\ &\quad \left. + \sum_{\sigma} \sum_{\mathbf{k}_{\sigma}} \frac{|V_{\mathbf{k}\Gamma\sigma}|^2}{N_L} e^{-\beta E_0} \int d\omega' e^{-\beta\omega'} C(\omega') \right] \end{aligned}$$

$$\times \int d\omega \frac{-1}{\pi} \text{Im} G_{\mathbf{k}\sigma}(\omega_+) \cdot \frac{f(\omega)}{(\omega + \omega' - E_{i\Gamma} + \varepsilon_f)^2} \Big], \quad (3.1)$$

$$\langle \hat{n}_{bi} \rangle_\lambda = e^{-\beta(\lambda_i + \varepsilon_f - E_0)} \times \left[a + e^{-\beta E_0} \int d\omega e^{-\beta\omega} C(\omega) \right], \quad (3.2)$$

where $a \equiv a(0)$. At $T = 0$, $\exp(-\beta E_0)$ vanishes for $E_0 > 0$, so that

$$\begin{aligned} \langle \hat{n}_{fi\Gamma} \rangle_\lambda &= e^{-\beta(\lambda_i + \varepsilon_f - E_0)} \sum_\sigma \sum_{\mathbf{k}\sigma} \frac{a|V_{\mathbf{k}\Gamma\sigma}|^2}{N_L} \int d\omega \frac{-1}{\pi} \text{Im} G_{\mathbf{k}\sigma}(\omega_+) \\ &\times \frac{f(\omega)}{(\omega - E_0 - E_{i\Gamma} + \varepsilon_f)^2}, \end{aligned} \quad (3.3)$$

$$\langle \hat{n}_{bi} \rangle_\lambda = a e^{-\beta(\lambda_i + \varepsilon_f - E_0)}. \quad (3.4)$$

Similarly, when we use eqs. (2.37), (2.43), and (2.44) at $T = 0$, the continuum part of the spectrum of the slave-boson Green function $C(\omega)$ in eq. (2.54) can also be neglected, because the continuum part is smaller than the contribution from a pole by a factor of $\exp(-\beta E_0)$. As a result the self-energy of the conduction electron, eq. (2.37), and $\langle \hat{Q}_i \rangle_\lambda$, (2.39), are given as

$$\begin{aligned} \langle \hat{Q}_i \rangle_\lambda &= a(1/a - 1) e^{-\beta(\lambda_i + \varepsilon_f - E_0)} + a e^{-\beta(\lambda_i + \varepsilon_f - E_0)}, \\ &= e^{-\beta(\lambda_i + \varepsilon_f - E_0)}, \end{aligned} \quad (3.5)$$

$$\Sigma_{\mathbf{k}\sigma}(\omega_+) = \sum_{\Gamma\pm} \frac{a|V_{\mathbf{k}\Gamma\sigma}|^2}{\omega_+ - E_0 - E_{i\Gamma} + \varepsilon_f}, \quad (3.6)$$

where we have used the relations eqs. (2.38) and (2.49). Here, we note that the self-energy $\Sigma_{\mathbf{k}\sigma}(\omega)$ of the conduction electrons does not have an imaginary part at $\omega = \mu = 0$. Hence a quasi-particle band is formed and the system behaves as a Fermi liquid, so that the Landau-Luttinger sum-rule holds, as seen in the previous section. From eq. (2.7), we rewrite eq. (3.6) as follows:

$$\text{Re} \Sigma_{\mathbf{k}\sigma}(\omega_+) = \sum_{\pm} \left[\frac{a|V_{\mathbf{k}|\pm 3}\sigma|^2}{\omega_+ - E_0} + \frac{a|V_{\mathbf{k}|\pm 2}\sigma|^2}{\omega_+ - E_0 - \Delta_1} + \frac{a|V_{\mathbf{k}|\pm 1}\sigma|^2}{\omega_+ - E_0 - \Delta_2} \right], \quad (3.7)$$

where, \sum_{\pm} means the summation over the Kramers doublets. We neglect the \mathbf{k} -dependence of $V_{\mathbf{k}\Gamma\sigma}$, and we assume the summation for $V_{\mathbf{k}\Gamma\sigma}$ over each of the Kramers doublets specified by Γ to be constant, i.e., $\sum_{\pm} |V_{\mathbf{k}\Gamma\sigma}|^2 = \sum_{\pm} |V_{\Gamma\sigma}|^2 = V^2$ for simplicity. However, this assumption does not qualitatively change the physical properties. Then, we obtain

$$\text{Re} \Sigma_{\mathbf{k}\sigma}(\omega_+) = \left[\frac{aV^2}{\omega_+ - E_0} + \frac{aV^2}{\omega_+ - E_0 - \Delta_1} + \frac{aV^2}{\omega_+ - E_0 - \Delta_2} \right], \quad (3.8)$$

$$\begin{aligned} G_{\mathbf{k}\sigma}(\omega_+) &= \frac{1}{\omega_+ - \varepsilon_{\mathbf{k}\sigma} - \Sigma_{\mathbf{k}\sigma}(\omega)}, \\ &= \sum_{j=1}^4 \frac{A_{\mathbf{k}}^j}{\omega_+ - \alpha_{\mathbf{k}\sigma}^j}, \end{aligned} \quad (3.9)$$

where $\alpha_{\mathbf{k}\sigma}^j$ and $A_{\mathbf{k}}^j$, defined by the pole and residue of the Green function of the conduction electron, must satisfy the following equations

$$\alpha_{\mathbf{k}\sigma}^j - \varepsilon_{\mathbf{k}\sigma} - \text{Re}\Sigma_{\mathbf{k}\sigma}(\alpha_{\mathbf{k}\sigma}^j) = 0, \quad (3.10)$$

and

$$A_{\mathbf{k}}^j = \frac{(\alpha_{\mathbf{k}\sigma}^j - E_0)(\alpha_{\mathbf{k}\sigma}^j - E_0 - \Delta_1)(\alpha_{\mathbf{k}\sigma}^j - E_0 - \Delta_2)}{(\alpha_{\mathbf{k}\sigma}^j - \alpha_{\mathbf{k}\sigma}^{j+1})(\alpha_{\mathbf{k}\sigma}^j - \alpha_{\mathbf{k}\sigma}^{j+2})(\alpha_{\mathbf{k}\sigma}^j - \alpha_{\mathbf{k}\sigma}^{j+3})}, \quad (3.11)$$

where $\alpha_{\mathbf{k}\sigma}^j = \alpha_{\mathbf{k}\sigma}^{j+4}$. The physical meaning of $\alpha_{\mathbf{k}\sigma}^j$ is the quasi-particle dispersion of the Fermi liquid, because the conduction electrons hybridize with the physical f-electron through the self-energy $\Sigma_{\mathbf{k}\sigma}$. E_0 and a in eq. (3.8) are determined by eqs. (2.48) and (2.49). The total number n ($= n_c + n_f$) per site is determined by eqs. (2.55) and (2.56).

$$E_0 - \varepsilon_f = \frac{1}{N_L} \sum_{j=1}^4 \sum_{\Gamma_{\pm}} \sum_{\sigma} \sum_{\mathbf{k}\sigma} \frac{A_{\mathbf{k}}^j |V_{\Gamma\sigma}|^2 f(\alpha_{\mathbf{k}\sigma}^j)}{E_0 + E_{i\Gamma} - \varepsilon_f - \alpha_{\mathbf{k}\sigma}^j}, \quad (3.12)$$

$$\frac{1}{a} = 1 + \frac{1}{N_L} \sum_{j=1}^4 \sum_{\Gamma_{\pm}} \sum_{\sigma} \sum_{\mathbf{k}\sigma} \frac{A_{\mathbf{k}}^j |V_{\Gamma\sigma}|^2 f(\alpha_{\mathbf{k}\sigma}^j)}{(E_0 + E_{i\Gamma} - \varepsilon_f - \alpha_{\mathbf{k}\sigma}^j)^2}, \quad (3.13)$$

$$n = n_c + n_f = \frac{1}{N_L} \sum_{j=1}^4 \sum_{\sigma} \sum_{\mathbf{k}\sigma} f(\alpha_{\mathbf{k}\sigma}^j) A_{\mathbf{k}}^j + (1 - a). \quad (3.14)$$

Here, n_f is also derived from $1 - a$ because of local constraints eq. (2.9), where a is defined as a residue of the slave-boson Green function in eq. (2.54). At $T = 0$, the residue a is equivalent to the number of f^0 -states per site: i.e., $n_f = 1 - a$. By solving a set of self-consistent equations (3.12)~(3.14), we can obtain physical quantities at $T = 0$. The solution derived from the above equations is consistent with that of slave-boson mean field theory at $T = 0$. In the following subsections, we show the numerical results.

3.1 Dispersion of renormalized band

We assume that the dispersion of the bare conduction electrons is linear in any direction, so that the DOS of the conduction electron per spin is approximated as follows:

$$\rho_{\sigma}(\omega) \equiv -\frac{1}{\pi} \frac{1}{N_L} \sum_{\mathbf{k}\sigma} \text{Im}G_{\mathbf{k}\sigma}^0(\omega_+), \quad (3.15)$$

$$\rho_{\sigma}(\omega) = \begin{cases} \rho_0 = \frac{1}{2D} & (-D \leq \omega \leq D), \\ 0 & (\text{otherwise}). \end{cases} \quad (3.16)$$

We adopt the following parameters; $D = 1$, $n \equiv n_c + n_f = 1.4$, $V^2 = 0.02D^2$, $\varepsilon_f^{(0)} = -0.7D$, where $\varepsilon_f^{(0)}$ is defined as the energy level of f-electrons measured from the center of the conduction electron band, and $\varepsilon_f \equiv \varepsilon_f^{(0)} - \mu$. Although one might think that the parameter V has too small a value, the binding energy of the slave-boson E_0 is found to be $E_0 \sim 0.01D$ in the case of $\Delta_1 = \Delta_2 = 0$ under these parameters.

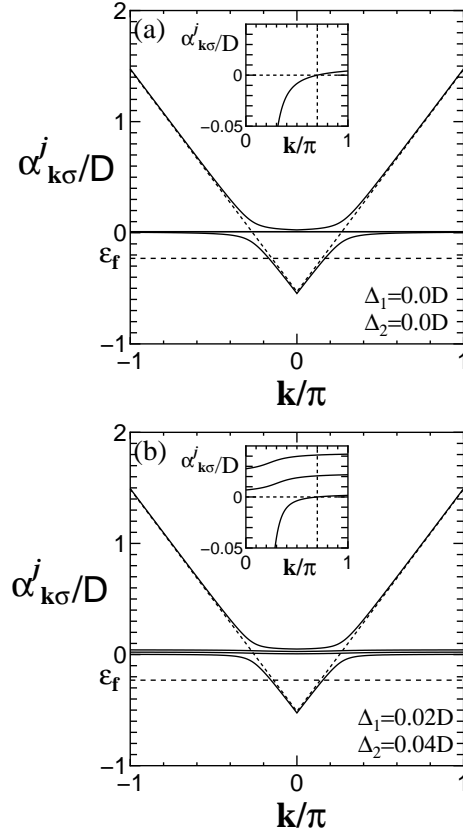


Fig. 7. Schematic structure of the renormalized bands $\alpha_{k\sigma}^j$ for the Fermi level set to zero. ϵ_f is the atomic f-level measured from the Fermi level. Δ_1 and Δ_2 are CEF splittings ($\Delta_1 \leq \Delta_2$).

We show the dispersion of renormalized bands $\alpha_{k\sigma}^j$, given by the solution of (3.10), for two cases of Δ_1 and Δ_2 in Fig. 7(a) and (b), where the Fermi level is set to be zero. In the absence of CEF splitting (Fig. 7(a)), the conduction electron mixes only with two linear combinations of 6-fold degenerate states of f-electrons, so that such a band consisting of two linear combinations is renormalized, and others remain un-renormalized. On the other hand, in the case of Fig. 7(b) where CEF splitting exists, the conduction band is renormalized by hybridizing with each f-level, so that the dispersion of the renormalized band is divided into four bands. The insets of Fig. 7(a) and (b) show that the Landau-Luttinger sum-rule holds because the Fermi wavenumber is fixed as $k_F = 0.7\pi$ corresponding to $n = n_c + n_f = 1.4$.

We display the relationship between E_0 and V^2 in Fig. 8(a), where other parameters are fixed at their previously given values. One can see that the characteristic temperature E_0 , which corresponds to the Kondo temperature in the impurity problem, increases with increase in the hybridization parameter. Since the effect of pressure is simulated by an increase in the hybridization parameter between the conduction electrons and the f-electrons, E_0 rises monotonously with increasing applied pressure. Fig. 8(b) shows the V^2 dependence of the

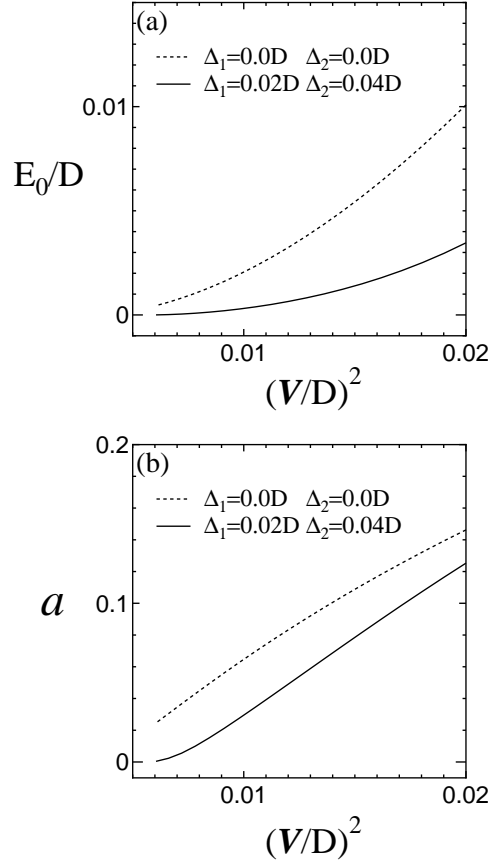


Fig. 8. (a) E_0 vs V^2 , and (b) a vs V^2 for $\Delta_1 = \Delta_2 = 0.0D$ (dotted line), and $\Delta_1 = 0.02D$ $\Delta_2 = 0.04D$ (solid line).

residue a of the slave-boson Green function. This shows that n_f ($= 1 - a$) approaches unity with decreasing V . This behavior is consistent with that of the renormalization factor q derived from a mean-field-type approximation¹⁸⁾ and a Variational Monte Carlo study¹⁹⁾ on the basis of the Gutzwiller ansatz:

$$q^{-1} = \frac{1 - n_f/2}{1 - n_f}. \quad (3.17)$$

3.2 Spectral weight of slave-boson

We calculate the spectral weight of the slave-boson at $T = 0$. The spectral function $\rho_b(\omega)$ of the slave-boson is given by

$$\rho_b(\omega) \equiv -\frac{1}{\pi} \text{Im} \bar{B}(\omega_+) = \frac{1}{\pi} \cdot \frac{0_+ - \text{Im} \bar{\Pi}(\omega_+)}{[\omega + \varepsilon_f - \text{Re} \bar{\Pi}(\omega_+)]^2 + [0_+ - \text{Im} \bar{\Pi}(\omega_+)]^2}. \quad (3.18)$$

We adopt following parameters; $D = 1$, $n \equiv n_c + n_f = 1.4$, $V^2 = 0.02D^2$, $\varepsilon_f^{(0)} = -0.7D$, and show the results in the absence of Δ_1 , Δ_2 and $\Delta_1 = 0.02D$, $\Delta_2 = 0.04D$ in Fig. 9 and 10. The

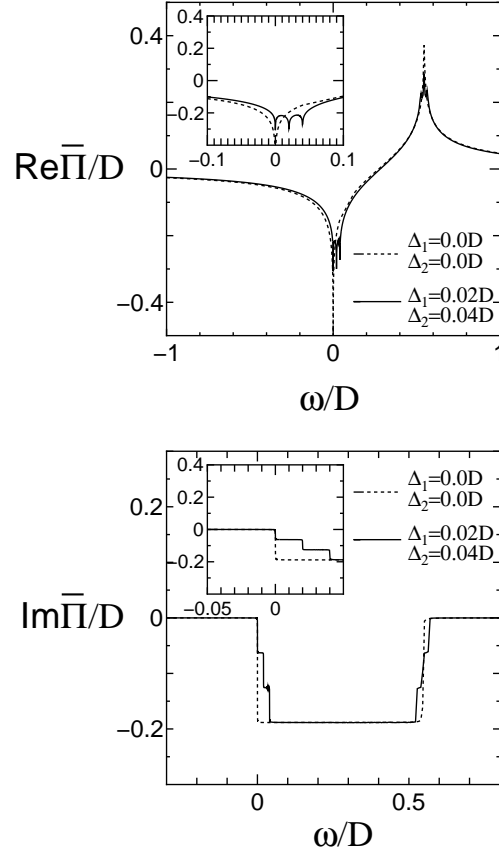


Fig. 9. Self-energy of the slave-boson $\bar{\Pi}(\omega)$ for the case of $\Delta_1 = \Delta_2 = 0$, and $\Delta_1 = 0.02D$ $\Delta_2 = 0.04D$. Insets show magnified section around $\omega = 0$.

function of the self-energy of the slave-boson $\bar{\Pi}(\omega)$ is illustrated in Fig. 9 for two sets of the CEF level scheme $\Delta_1 = \Delta_2 = 0$, and $\Delta_1 = 0.02D$ and $\Delta_2 = 0.04D$. At $T = 0$ in the absence of CEF splitting, $\text{Im}\bar{\Pi}(\omega)$ has a sharp structure at $\omega = 0$ due to the Fermi distribution function, i.e., from eq. (2.51)

$$\text{Im}\bar{\Pi}(\omega_+) = \frac{3V^2}{N_L} \sum_{\sigma} \sum_{\mathbf{k}_{\sigma}} f(-\omega) \text{Im}G_{\mathbf{k}\sigma}(-\omega + i0_+), \quad (3.19)$$

where we note that $E_{i\Gamma} = \varepsilon_f$ in the absence of CEF splitting in eq. (2.51). When we take into account the CEF splitting, three-step-like structure appears, because $\text{Im}\bar{\Pi}(\omega)$ is given by

$$\begin{aligned} \text{Im}\bar{\Pi}(\omega_+) = & \frac{V^2}{N_L} \sum_{\sigma} \sum_{\mathbf{k}_{\sigma}} \left[f(-\omega) \text{Im}G_{\mathbf{k}\sigma}(-\omega + i0_+) \right. \\ & \left. + \sum_{l=1,2} f(-\omega + \Delta_l) \text{Im}G_{\mathbf{k}\sigma}(-\omega + \Delta_l + i0_+) \right]. \end{aligned} \quad (3.20)$$

Fig. 10 shows the spectral function of the slave-boson $\rho_b(\omega)$, for the same sets of the CEF level scheme. One can see that the resonant peak is exhibited at $\omega = E_0$ and a broad continuum appears in the region of $\omega > 0$. The condition, $\omega + \varepsilon_f - \text{Re}\bar{\Pi}(\omega) = 0$, is satisfied

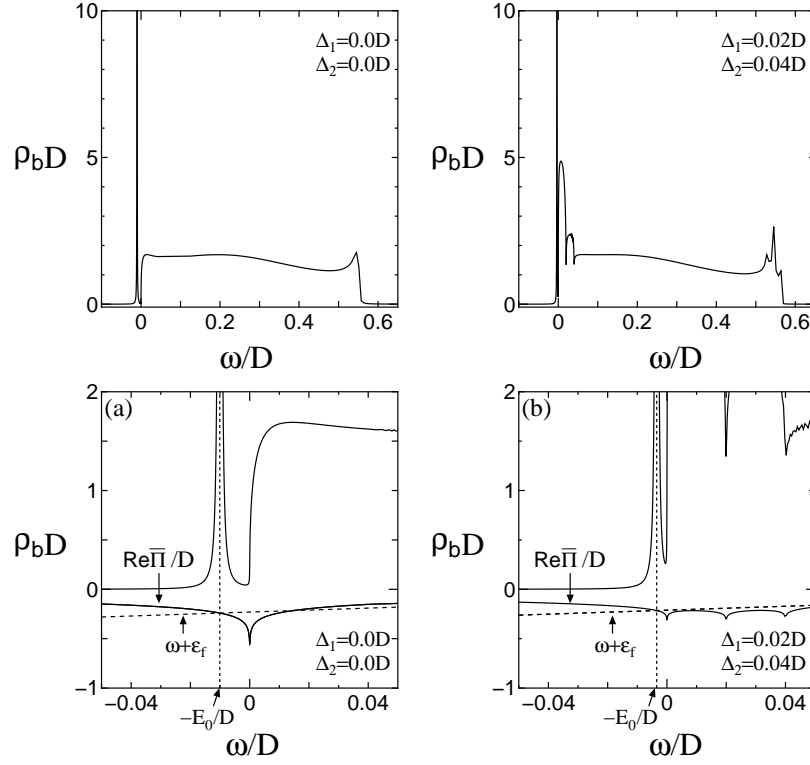


Fig. 10. Spectral function $\rho_b(\omega)$ of the slave-boson. In panels (a) and (b), the region $\omega \sim 0$ is enlarged, and the real part of $\bar{\Pi}(\omega)$ is also shown.

only when $\omega = -E_0$ ($E_0 > 0$) in the region of $\omega < 0$ in Fig. 10, while $\text{Im}\bar{\Pi}(\omega) = 0$ at $\omega < 0$ in Fig. 9. For this reason, $\rho_b(\omega)$ has a resonant peak at $\omega = -E_0$, such as $1/(\omega + E_0 + i0_+)$. In the region of $0 < \omega < \omega_{\text{edge}}$, where ω_{edge} is defined by a condition $\text{Im}G_{\mathbf{k}\sigma}(\omega \geq \omega_{\text{edge}}) = 0$, $\text{Im}\bar{\Pi}$ has a finite value in Fig. 9, so that $\rho_b(\omega)$ has a broad peak in this region. This result is consistent with eq. (2.54).

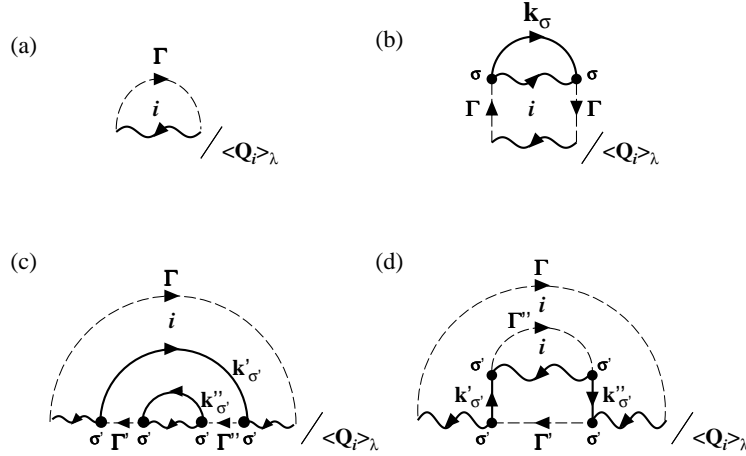
3.3 Spectral weight of conduction electron and f-electron

Next, we calculate the one-particle spectral weight $\rho_c(\omega)$ of the conduction electron and $\rho_f^i(\omega)$ of the f-electron. The spectral weight $\rho_c(\omega)$ is defined by

$$\begin{aligned} \rho_c(\omega) &\equiv \frac{1}{N_L} \sum_{\sigma} \sum_{\mathbf{k}\sigma} \rho_{\mathbf{k}\sigma}(\omega) = \frac{1}{N_L} \sum_{\sigma} \sum_{\mathbf{k}\sigma} \left[\frac{-1}{\pi} \text{Im}G_{\mathbf{k}\sigma}(\omega_+) \right], \\ &= \frac{1}{N_L} \sum_{\sigma} \sum_{\mathbf{k}\sigma} \left[\sum_{j=1}^4 A_{\mathbf{k}}^j \cdot f(\alpha_{\mathbf{k}\sigma}^j) \right], \end{aligned} \quad (3.21)$$

and the spectral weight $\rho_f^i(\omega)$ of f-electrons is as follows:

$$\rho_f^i(\omega) \equiv -\frac{1}{\pi} \lim_{\lambda_i \rightarrow \infty} \left[\sum_{\Gamma_{\pm}} \text{Im}G_{f\Gamma}^{i,\lambda}(\omega_+) / \langle \hat{Q}_i \rangle_{\lambda} \right], \quad (3.22)$$

Fig. 11. Lowest order contribution to G_f^i in $1/N$ -expansion.

$$= -\frac{1}{\pi} \left[\text{Im} G_f^i(\omega_+) \right], \quad (3.23)$$

where

$$G_{f\Gamma}^{i,\lambda}(i\omega_n) \equiv - \int_0^\beta e^{i\omega_n \tau} \langle T\tau [f_{i\Gamma}(\tau) b_i^\dagger(\tau) b_i f_{i\Gamma}^\dagger] \rangle_\lambda d\tau, \quad (3.24)$$

$$G_f^i(\omega_+) = \lim_{\lambda_i \rightarrow \infty} \sum_{\Gamma_\pm} G_{f\Gamma}^{i,\lambda}(\omega_+) / \langle \hat{Q}_i \rangle_\lambda = \sum_{\Gamma_\pm} G_{f\Gamma}^i(\omega_+). \quad (3.25)$$

Here, it is noted that the annihilation operator $f_{\text{phys},i}$ of the physical f-electron at the i -th site is given by the product of the operators of the pseudo-fermion and the slave-boson as $f_{\text{phys},i} = f_{i\Gamma} b_i^\dagger$. Namely, the Green function G_f^i for f-electron is obtained by the convolution of slave-boson and pseudo-fermion Green function. The lowest order contribution to G_f^i in the $1/N$ -expansion is illustrated in Fig. 11. The diagrams (b), (c), (d) in Fig. 11, when the summations on σ were not performed, give higher order corrections to the self-energy of the conduction electron, according to the classification rule of the Feynman diagrams in §2. However, when we calculate the spectral weight, an extra summation with respect to σ must be performed, so that the terms are returned to the lowest contributions. The first term (a) in Fig. 11, which is denoted as $G_f^i(\omega_+)_{(a)}$, is given as follows:

$$G_{f\Gamma}^i(i\omega_n)_{(a)} = - \lim_{\lambda_i \rightarrow \infty} \sum_{\Gamma_\pm} T \sum_{\nu_n} B_i(i\nu_n) F_{i\Gamma}^0(i\omega_n + i\nu_n) / \langle \hat{Q}_i \rangle_\lambda, \quad (3.26)$$

where $B_i(i\nu_n)$ and $F_{i\Gamma}^0(i\omega_n + i\nu_n)$ are given by eqs. (2.17) and (2.18), respectively. The convolution of B_i and $F_{i\Gamma}^0$, eq. (3.26), is equal to $\Sigma_{\mathbf{k}\sigma} / |V_{\mathbf{k}\Gamma\sigma}|^2$ as can be seen in eq. (2.37) if the \mathbf{k} -dependence of $V_{\mathbf{k}\Gamma\sigma}$ is neglected as in the present approximation scheme. On this basis, with the use of eq. (3.6) for $\Sigma_{\mathbf{k}\sigma}$, we obtain

$$G_f^i(\omega_+)_{(a)} = \sum_{\Gamma_\pm} \frac{a}{\omega_+ - E_0 - E_{i\Gamma} + \varepsilon_f}. \quad (3.27)$$

Then, a contribution to the average number from $G_f^i(\omega)_{(a)}$ is

$$\int d\omega f(\omega) \left[\frac{-1}{\pi} \text{Im} G_f^i(\omega)_{(a)} \right] = \sum_{\Gamma_{\pm}} a f(E_0 + E_{i\Gamma} - \varepsilon_f) = 0, \quad (3.28)$$

where $E_0 > 0$, so that $E_0 + E_{i\Gamma} - \varepsilon_f > 0$. $\text{Im} G_f^i(\omega)_{(a)}$ has a value only in the region of $\omega > 0$. Therefore, the contribution from the first term (a) in Fig. 11 vanishes. The terms (c) and (d) in Fig. 11 also have a value only in the region of $\omega > 0$, so that they do not contribute to the average number of f-electrons. As a result only the second term (b) in Fig. 11 has a value in the region of $\omega < 0$ and contributes to the average number of f-electrons at $T = 0$. For this reason, when we discuss the spectral weight of the f-electron in the region of $\omega < 0$ at $T = 0$, we should only take into account term (b). The analytical form of the second term (b) at $T = 0$ is given by (See Appendix A for details)

$$\begin{aligned} G_f^i(\omega)_{(b)} &= \frac{1}{N_L} \sum_{\Gamma_{\pm}} \sum_{\sigma} \sum_{\mathbf{k}_{\sigma}} |V_{\Gamma\sigma}|^2 \int d\varepsilon f(\varepsilon) \left[\frac{-1}{\pi} \text{Im} G_{\mathbf{k}\sigma}(-\varepsilon + i0_+) \right] \int d\varepsilon' e^{-\beta(E_0 + \varepsilon')} \\ &\quad \times \left[\frac{-1}{\pi} \text{Im} \bar{B}(\varepsilon' + i0_+) \right] \bar{B}(\omega + \varepsilon + \varepsilon') \frac{1}{(\omega + \varepsilon' - E_{i\Gamma} + \varepsilon_f)^2} / \langle \hat{Q} \rangle \\ &\quad + \frac{1}{N_L} \sum_{\Gamma_{\pm}} \sum_{\sigma} \sum_{\mathbf{k}_{\sigma}} |V_{\Gamma\sigma}|^2 \int d\varepsilon f(\varepsilon) \left[\frac{-1}{\pi} \text{Im} G_{\mathbf{k}\sigma}(\varepsilon + i0_+) \right] \int d\varepsilon' e^{-\beta(E_0 + \varepsilon')} \\ &\quad \times \left[\frac{-1}{\pi} \text{Im} \bar{B}(\varepsilon' + i0_+) \right] \bar{B}(-\omega + \varepsilon + \varepsilon' + i0_+) \frac{1}{(\varepsilon + \varepsilon' - E_{i\Gamma} + \varepsilon_f)^2} / \langle \hat{Q} \rangle, \end{aligned} \quad (3.29)$$

where we have used the previous notation: $\langle \hat{Q}_i \rangle_{\lambda} = e^{-\beta(\lambda_i + \varepsilon_f - E_0)} \langle \hat{Q} \rangle$. Substituting this into eq. (3.23), we obtain

$$\begin{aligned} \rho_f^i(\omega) &= \frac{1}{N_L} \sum_{\Gamma_{\pm}} \sum_{\sigma} \sum_{\mathbf{k}_{\sigma}} |V_{\Gamma\sigma}|^2 \int d\varepsilon f(\varepsilon) \int d\varepsilon' e^{-\beta(E_0 + \varepsilon')} \frac{-1}{\pi} \text{Im} \bar{B}(\varepsilon' + i0_+) / \langle \hat{Q} \rangle \\ &\quad \times \left[\frac{-1}{\pi} \text{Im} G_{\mathbf{k}\sigma}(-\varepsilon + i0_+) \cdot \frac{-1}{\pi} \text{Im} \bar{B}(\omega + \varepsilon + \varepsilon' + i0_+) \cdot \frac{1}{(\omega + \varepsilon' - E_{i\Gamma} + \varepsilon_f)^2} \right. \\ &\quad \left. + \frac{-1}{\pi} \text{Im} G_{\mathbf{k}\sigma}(\varepsilon + i0_+) \cdot \frac{-1}{\pi} \text{Im} \bar{B}(-\omega + \varepsilon + \varepsilon' + i0_+) \cdot \frac{1}{(\varepsilon + \varepsilon' - E_{i\Gamma} + \varepsilon_f)^2} \right]. \end{aligned} \quad (3.30)$$

With the use of (2.54) at $T = 0$, this is reduced to

$$\rho_f^i(\omega) = \sum_{\Gamma_{\pm}} \sum_{\sigma} \left(\frac{a|V_{\Gamma\sigma}|}{\omega - E_0 - E_{i\Gamma} + \varepsilon_f} \right)^2 \rho_{\sigma}(\omega) \quad (3.31)$$

$$+ \sum_{\Gamma_{\pm}} \sum_{\sigma} \frac{a|V_{\Gamma\sigma}|^2}{(\omega - E_0 - E_{i\Gamma} + \varepsilon_f)^2} \int d\varepsilon f(\varepsilon) \rho_{\sigma}(-\varepsilon) C(\omega + \varepsilon - E_0) \quad (3.32)$$

$$+ \sum_{\Gamma_{\pm}} \sum_{\sigma} \int d\varepsilon f(\varepsilon) \rho_{\sigma}(\varepsilon) C(-\omega + \varepsilon - E_0) \frac{a|V_{\Gamma\sigma}|^2}{(\varepsilon - E_0 - E_{i\Gamma} + \varepsilon_f)^2}. \quad (3.33)$$

Here, ρ_{σ} is defined in eq. (3.15), and $C(\omega)$ is the broad continuous function in eq. (2.54). The contribution from eq. (3.31) corresponds to the coherent part of the spectral weight of f-electrons, and that from eqs. (3.32) and (3.33) give its incoherent part.

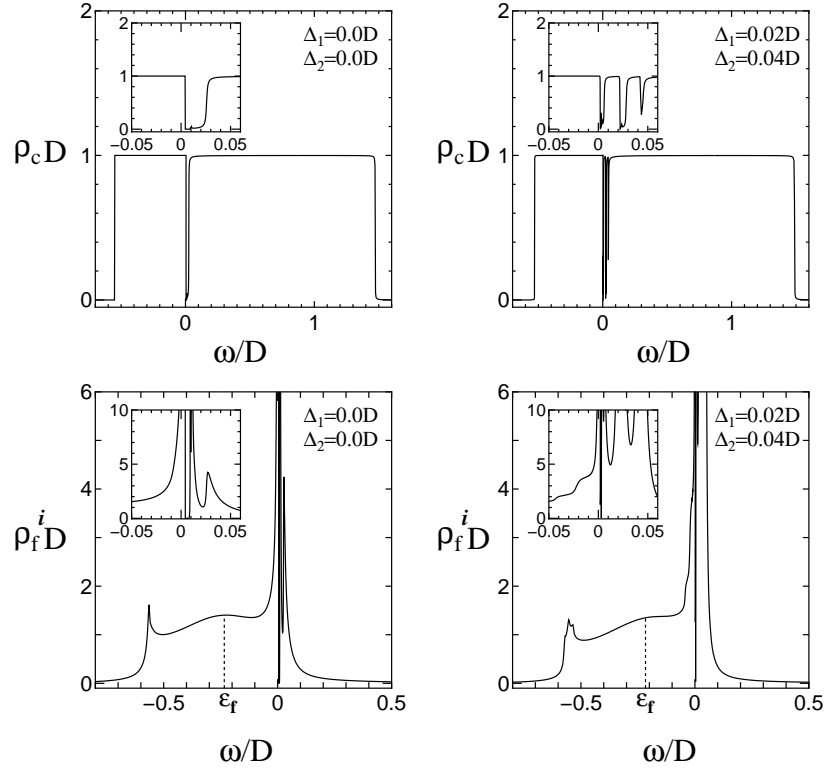


Fig. 12. Spectral weight of the conduction electron and f-electron. Insets are magnified views around $\omega = 0$.

We show the numerical results of $\rho_c(\omega)$, eq. (3.21), and $\rho_f^i(\omega)$, eqs. (3.31)~(3.33), in Fig. 12, where we adopt the following parameters: $D = 1$, $n \equiv n_c + n_f = 1.4$, $V^2 = 0.02D^2$, $\varepsilon_f^{(0)} = -0.7D$. A resonance-like peak is observed at $\omega = E_0$ in $\rho_f^i(\omega)$, the spectrum of the f-electron. This peak arises from the term, eq. (3.32), in which $C(\omega)$ is a broad function of $\rho_b(\omega)$ in the region of $\omega > 0$. Physically speaking, it reflects a excitation process from the binding state of the slave-boson to continuum states whose minimum excitation energy is given by E_0 . This result can not be obtained by a simple quasi-particle picture of the Fermi liquid, where the renormalization factor z is estimated as $z = (1 - \partial\Sigma(\omega)/\partial\omega|_{\omega=0})^{-1}$, but is related to a subtle structure of incoherent states with excitation energy of the order $E_0 \sim T_F^*$, T_F^* being a renormalized Fermi energy. Here, with the use of these spectral weight functions, we find that the following sum-rule holds within an error of a few percentage at worse.

$$\int_{-\infty}^{\infty} d\omega f(\omega) \left[\rho_c(\omega) + \rho_f^i(\omega) \right] = n. \quad (3.34)$$

3.4 Kondo temperature

E_0 defined as the binding energy of the slave-boson at $T = 0$ corresponds to the Kondo temperature T_K defined in an impurity version of the Anderson model. In the impurity problem, the conduction electron is not renormalized, so that we can put $E_0 \rightarrow T_K$, $\alpha_{\mathbf{k}\sigma}^j \rightarrow \varepsilon_{\mathbf{k}\sigma}$

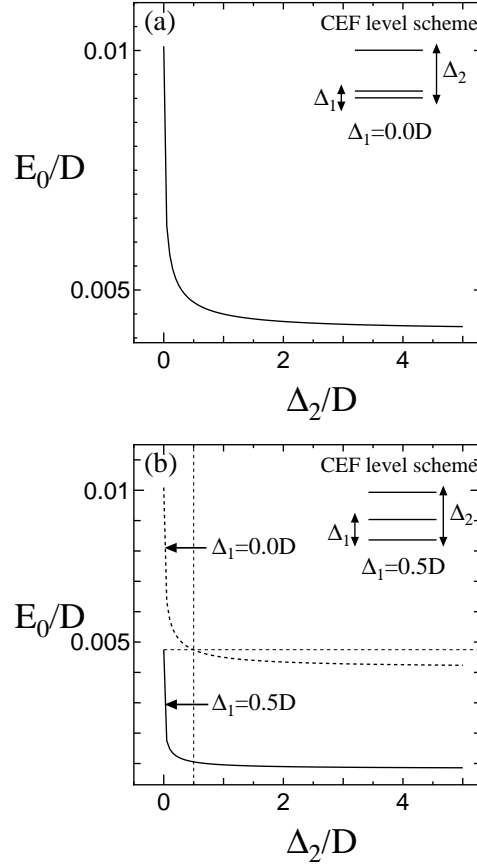


Fig. 13. (a) Δ_2 vs E_0 in the case of $\Delta_1 = 0$. (b) Δ_2 vs E_0 in the both case of $\Delta_1 = 0$ (dot line) and $\Delta_1 = 0.5D$ (solid line).

and $A_{\mathbf{k}}^j \rightarrow 1$. Then, we only have to take into account eq. (3.12), leading to

$$T_K = D \cdot \left(\frac{D}{\Delta_1}\right) \cdot \left(\frac{D}{\Delta_2}\right) \exp\left(-\frac{|\varepsilon_f|}{2\rho_0 V^2}\right). \quad (3.35)$$

Similarly, we can calculate the Kondo temperature $T_K^{(0)}$ in the absence of CEF splitting. Then, we can derive the following relation between T_K and $T_K^{(0)}$ under the condition $T_K \ll \Delta_1 \sim \Delta_2 \ll |\varepsilon_f| < |D|$,

$$\left[T_K^{(0)}\right]^3 = \Delta_1 \cdot \Delta_2 \cdot T_K. \quad (3.36)$$

(See Appendix B for derivation) This result is consistent with previous works on the impurity problem.^{20,21)}

Next, we consider the lattice problem, for which we must solve coupled self-consistent equations (3.12)~(3.14). By solving these equations, we can evaluate E_0 , which is regarded as the Kondo temperature in the lattice case. We illustrate the numerical results for the effect of CEF splitting on E_0 in Fig. 13, where we adopt the following parameters; $D = 1$, $n \equiv n_c + n_f = 1.4$, $V^2 = 0.02D^2$, $\varepsilon_f^{(0)} = -0.7D$, and (a) $\Delta_1 = 0.0D$, and (b) $\Delta_1 = 0.5D$.

In case (a), if $\Delta_2 = 0.0D$, E_0 should be in agreement with $E_0^{(0)}$, which is defined as the Kondo temperature in the absence of CEF splitting in the lattice case. Here, with the use of the relations (3.35) and (3.36) derived in the impurity case, we can roughly estimate $E_0^{(0)}$ from $T_K^{(0)}$. Substituting the present set of parameters: $\rho_0 = 0.5/D$, $\varepsilon_f \equiv \varepsilon_f^{(0)} - \mu = -0.23D$, and $V^2 = 0.02D^2$, we obtain

$$T_K^{(0)} = D \exp\left(-\frac{0.23}{6 \times 0.5 \times 0.02}\right) \simeq 2.16 \times 10^{-2}D. \quad (3.37)$$

Numerical results in Fig. 13(a) show $E_0^{(0)} \sim 10^{-2}D$, which is reasonable compared with the rough estimate of eq. (3.37).

One can see in Fig. 13(a) that E_0 decreases rapidly with increasing Δ_2 , and E_0 saturates at $\Delta_2 \simeq 4D$. This shows that the Kondo temperature shifts from that with 6-fold degeneracy to that with 4-fold degeneracy. Such a behavior was not derived from the $SU(N)$ -PAM+CEF model, in which E_0 becomes a negative value at large $\Delta \sim 4D$. Namely, the application of the $1/N$ -expansion method to $SU(N)$ -PAM fails when we take into account the CEF splitting.

In case (b), E_0 also decreases rapidly with increasing Δ_2 as shown in Fig. 13(b). This also shows that the Kondo temperature shifts from that with 4-fold degeneracy to that with 2-fold degeneracy. We find that the value of $E_0 \sim 4.7 \times 10^{-3}D$ at $\Delta_1 = 0.0D$, $\Delta_2 = 0.5D$ is consistent with that of E_0 at $\Delta_1 = 0.5D$, $\Delta_2 = 0.0D$.

4. Physical properties at Finite Temperatures

In this section, we discuss the resistivity over the entire temperature range. To this end, we perform the calculations beyond the low-temperature approximation given in §3. In other words, when we discuss the physical properties at high temperatures ($T \gg E_0$), it is not appropriate to use eq. (2.54) given in §3, since $\text{Im}\bar{\Pi}$ has the width of $\sim T$ near $\omega = 0$ due to the thermal smearing effect of the Fermi distribution function. Namely, the picture of the resonant peak at E_0 ceases to be valid so that we must take into account the entire structure of the spectrum of the slave-boson and the contribution from the pole of pseudo-fermion at high temperatures. Then, we must solve the Dyson equations eqs. (2.16)~(2.18) for the single-particle Green functions self-consistently for all values of frequency ω at each temperature. Details of the self-consistent calculation are discussed in Appendix C.

4.1 Spectral weight of conduction electron

The spectral weight of $\rho_c(\omega)$ of the conduction electron, given by eq. (3.21), is shown in Fig. 14 for a series of temperatures. The parameters adopted are the same as for Fig. 14~Fig. 19: $D = 1$, $n \equiv n_c + n_f = 1.4$, $V^2 = 0.02D^2$, $\varepsilon_f^{(0)} = -0.7D$. Fig. 14(a) is for the case without CEF splitting ($\Delta_1 = \Delta_2 = 0$), and Fig. 14(b) is for the case with CEF splitting $\Delta_1 = 0.02D$ and $\Delta_2 = 0.04D$. Here, we have also assumed the DOS of bare conduction electron per spin

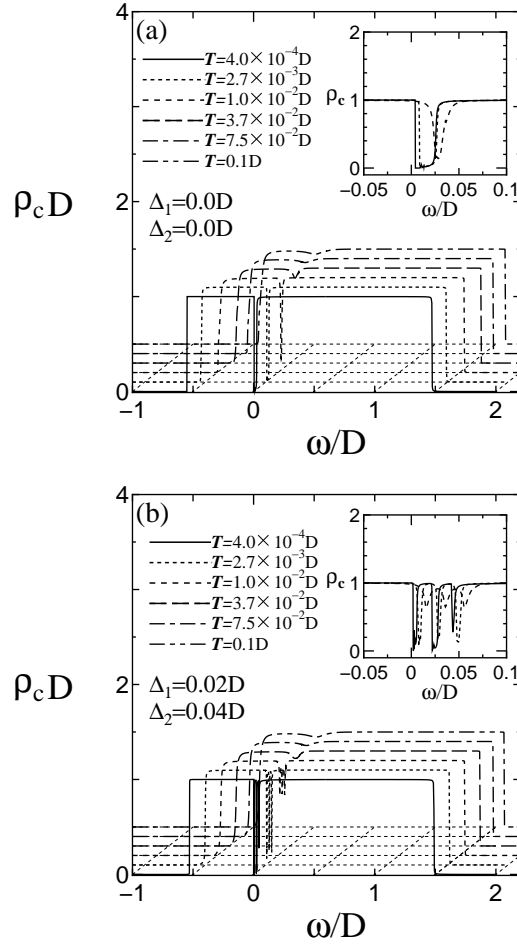


Fig. 14. Spectral weight of conduction electron at each temperature for cases (a) $\Delta_1 = \Delta_2 = 0.0D$ and (b) $\Delta_1 = 0.02D$ $\Delta_2 = 0.04D$. Insets are magnified views around $\omega = 0$.

as follows:

$$\rho_\sigma(\omega) = \frac{1}{N_L} \sum_{\mathbf{k}\sigma} \rho_{\mathbf{k}\sigma} = \begin{cases} \rho_0 = \frac{1}{2D} & (-D \leq \omega \leq D), \\ 0 & (\text{otherwise}). \end{cases} \quad (4.1)$$

With increasing temperature, the hybridization gap in the spectral weight of the conduction electron is gradually buried through pseudo-gap-like behavior. Such behavior has already been pointed out in a previous work detailed in ref. 10. It is noted that, in the case of $\Delta_1 = 0.02D$ and $\Delta_2 = 0.04D$, three hybridization gaps, corresponding to each CEF level, appear in the low-temperature limit.

4.2 Spectral weight of slave boson

In Fig. 15, we show the spectral function of the slave-boson in the case without CEF splitting, i.e., $\Delta_1 = \Delta_2 = 0.0D$. In the finite temperature calculation, $E_0(T)$ is determined by the peak position of the spectral function of the slave-boson. In Fig. 15(a), we find that

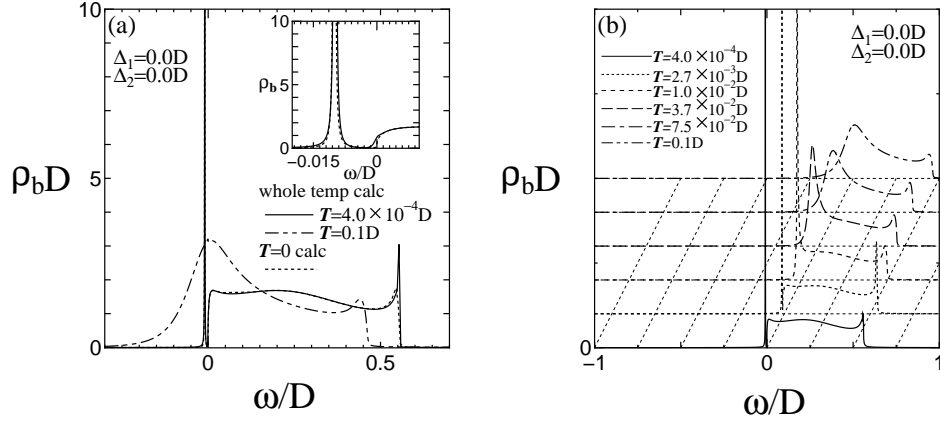


Fig. 15. (a) Spectral weight of slave-boson $\rho_b(\omega)$. Inset shows magnified view around $\omega = 0$. (b) $\rho_b(\omega)$ for a series of temperatures.

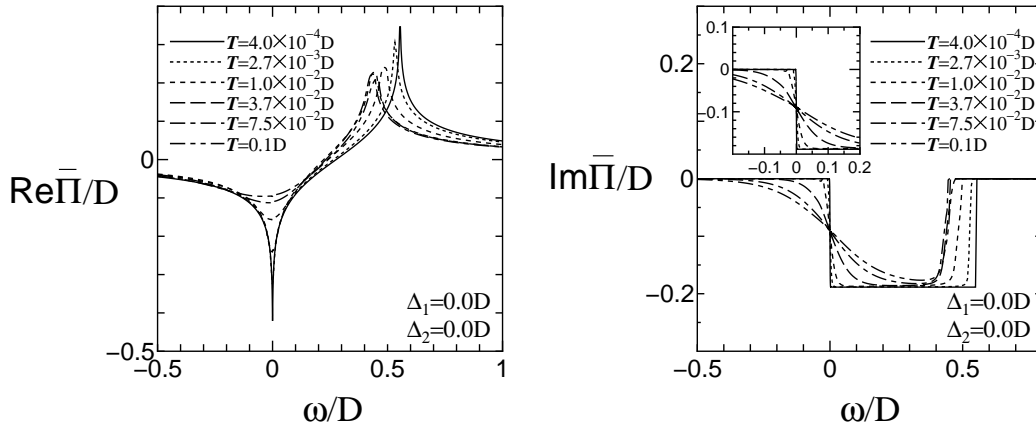


Fig. 16. Self-energy of slave-boson, $\text{Re}\bar{\Pi}(\omega)$ and $\text{Im}\bar{\Pi}(\omega)$, for a series of temperatures. Inset is magnified view around $\omega = 0$.

$E_0(4 \times 10^{-4}D)$ is almost the same as the result $E_0(0)$ derived from the $T = 0$ calculation in §3, $E_0(0) \simeq 0.01$. Namely, we can confirm that our calculation is performed from a low temperature ($T \lesssim T_0$) to a high temperature ($T > E_0$) continuously. Furthermore, we find that at a high temperature such as $T = 0.1D$, the spectral weight of the slave-boson cannot be divided into the resonant peak and broad function like eq. (2.54).

In Fig. 15(b), we show the results for a series of temperatures $4 \times 10^{-4} < T/D < 0.1$. We find that the validity of eq. (2.54) collapses at $T \sim 0.01 \sim E_0(0)$. Indeed, the low-temperature approximation fails at temperatures higher than $E_0(0)/10$. In the case with CEF-splitting, such a behavior does not change essentially. However, $E_0(0)$ becomes smaller compared with the case of $\Delta_1 = \Delta_2 = 0.0D$ (See Fig. 8(a)), and a three-step-like structure appears due to the CEF-splitting (See Fig. 9 and 10).

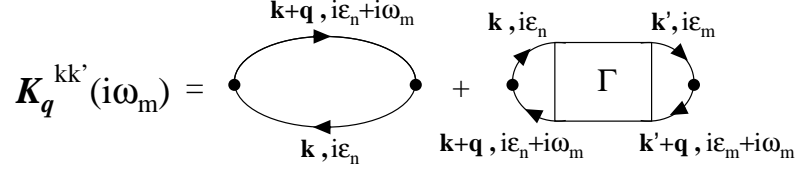


Fig. 17. Diagrammatic representation of the current-current response function.

Next, we show the result for the self-energy of the slave-boson in Fig. 16. $\text{Im}\bar{\Pi}(\omega)$ has a sharp structure around $\omega = 0$ at $T = 4 \times 10^{-4}D$, while its width broadens with increasing temperature due to the smearing effect of the Fermi distribution function. Therefore, $\text{Im}\bar{\Pi}(\omega)$ at high temperatures has a finite value even in the region of $\omega < 0$. Hence, the peak at $\omega = E_0$ has a finite width, so that $\rho_b(\omega)$ cannot be divided into two parts, a resonant peak (in the region of $\omega < 0$) and a broad background (in the region of $\omega > 0$), at high temperature $T \sim E_0$.

4.3 Electrical resistivity

In this subsection, the temperature dependence of the resistivity is discussed. We calculate the conductivity by means of the Kubo formula.²²⁾ Since the dispersion of f-electrons as well as the k -dependence of V is neglected, the conductivity is expressed by the Kubo formula

$$\sigma = \frac{e^2}{N_L^2} \sum_{\sigma} \sum_{\sigma'} \sum_{\mathbf{k}_{\sigma}} \sum_{\mathbf{k}'_{\sigma'}} v_{\mathbf{k}} v_{\mathbf{k}'} \lim_{q \rightarrow 0} \lim_{\omega \rightarrow 0} \frac{\text{Im} K_q^{\mathbf{k}\mathbf{k}'}(\omega_+)}{\omega}, \quad (4.2)$$

where $v_{\mathbf{k}} = \nabla_{\mathbf{k}} \varepsilon_{\mathbf{k}}$, K is a two-particle Green function defined as

$$K_q^{\mathbf{k}\mathbf{k}'}(\omega_+) = i \int_0^{\infty} dt e^{i\omega_+ t} \langle [c_{\mathbf{k}\sigma}^{\dagger}(t) c_{\mathbf{k}+\mathbf{q}\sigma}(t), c_{\mathbf{k}'\sigma'}^{\dagger}(0) c_{\mathbf{k}'-\mathbf{q}\sigma'}(0)] \rangle. \quad (4.3)$$

Since we are interested in the qualitative behavior of the resistivity, we neglect the vertex correction corresponding to the inverse collision process in the Landau-Boltzmann equation. However, the correction of the current vertex is taken into account through the Ward-Pitaevskii identity in the k -limit although this gives no net effect to the current vertex provided that the wave-number dependence of the self-energy $\Sigma_f(\mathbf{k}, \omega)$ of the f-electron can be neglected compared with its frequency dependence. Indeed, the Ward-Pitaevskii identity for the current vertex²³⁾ is given by

$$-\frac{\mathbf{p}}{m} + \frac{i}{2} \int \Gamma_{\alpha\beta, \alpha\beta}^{\mathbf{k}}(p, q) \frac{\mathbf{q}}{m} \{G^2(q)\}_{\mathbf{k}} \frac{d^4 q}{(2\pi)^4} = -\frac{\mathbf{p}}{m^* a'}, \quad (4.4)$$

where a' is the quasi-particle weight, and G is a one-particle Green function derived from the relation between the two-particle Green function and the vertex part. The right-hand side of eq. (4.4) can be approximated by $-\mathbf{p}/m$ if the k -dependence of Σ_f is neglected. By assuming implicitly that the Umklapp process works to violate the conservation of lattice momentum, the effect of collision is taken into account only through the self energy of $G_{\mathbf{k}\sigma}$. Then, $\text{Im}K$ is

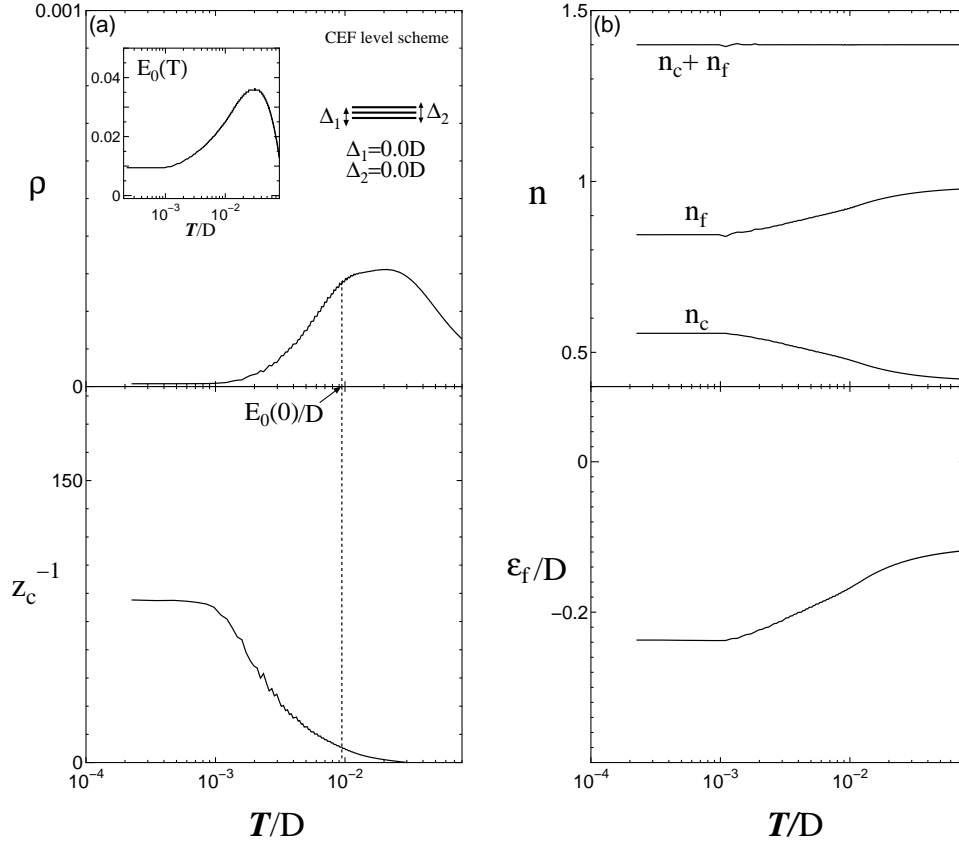


Fig. 18. (a) Temperature dependence of electrical resistivity $\rho(T)$ and z_c^{-1} . Inset is temperature dependence of E_0 . (b) Temperature dependences of number of conduction electrons n_c , f-electron n_f , and $n = n_c + n_f$, and ε_f measured from the chemical potential at a finite temperature.

given as (See Fig. 17)

$$\begin{aligned} \text{Im}K_q(\omega_+) = & -\delta_{\mathbf{k}\mathbf{k}'} \int d\varepsilon f(\varepsilon) \left[\frac{-1}{\pi} \text{Im}G_{\mathbf{k}\sigma}(\varepsilon + i0_+) \right] \\ & \times \text{Im} \left\{ G_{\mathbf{k}+\mathbf{q}\sigma}(\varepsilon + \omega + i0_+) - G_{\mathbf{k}+\mathbf{q}\sigma}(\varepsilon - \omega + i0_+) \right\}. \end{aligned} \quad (4.5)$$

Substituting this into eq. (4.2) and performing some rearrangements, we obtain

$$\sigma = \frac{e^2}{\pi N_L} \sum_{\sigma} \sum_{\mathbf{k}_{\sigma}} v_{\mathbf{k}}^2 \int d\varepsilon \left(-\frac{\partial f(\varepsilon)}{\partial \varepsilon} \right) \left[\text{Im}G_{\mathbf{k}\sigma}(\varepsilon + i0_+) \right]^2. \quad (4.6)$$

By omitting some constant factors, we define the reduced conductivity,

$$\tilde{\sigma} \equiv \frac{1}{N_L} \sum_{\sigma} \sum_{\mathbf{k}_{\sigma}} v_{\mathbf{k}}^2 \int d\varepsilon \left(-\frac{\partial f(\varepsilon)}{\partial \varepsilon} \right) \left[\text{Im}G_{\mathbf{k}\sigma}(\varepsilon + i0_+) \right]^2. \quad (4.7)$$

With the use of the renormalized Green function for $\text{Im}G_{\mathbf{k}\sigma}$ derived from §4.1, $\tilde{\sigma}$ is calculated numerically, and the reduced resistivity is defined as $\rho = \tilde{\sigma}^{-1}$. A result of the resistivity ρ is displayed in Fig. 18 and 19. In the absence of CEF splitting, the resistivity has a broad peak near $T \simeq 2E_0(0)$ as shown in Fig. 18(a). In the high-temperature region, $T > 2E_0(0)$,

the resistivity shows $-\log T$ behavior, typical of the Kondo effect. Here, we define the mass enhancement factor z_c as follows:

$$z_c^{-1} = 1 - \left. \frac{d\Sigma_{\mathbf{k}\sigma}(\omega)}{d\omega} \right|_{\omega=0_+}, \quad (4.8)$$

which is related to the quasi-particle weight $z_\Gamma = \left(1 - \left. \partial \Sigma_{i\Gamma}^f(\omega) / \partial \omega \right|_{\omega=0_+} \right)^{-1}$ as follows:

$$z_c^{-1} = 1 + \sum_{\Gamma\pm} |V_{\mathbf{k}\Gamma\sigma}|^2 G_{f\Gamma}^i(0)^2 z_\Gamma^{-1}, \quad (4.9)$$

where $G_{f\Gamma}^i(\omega_+)$ is defined in eq. (3.25). With decreasing temperature, z_c^{-1} begins to increase at around $T = E_0$ and saturates at a temperature lower than $T_0 \sim E_0/10$. Namely, the quasi-particle is formed at a temperature lower than $T_0/10$. The resistivity ρ exhibits a gradual decrease in this temperature region. In the present calculation of the leading order in $1/N$, in which the inter-site correlation of f-electrons cannot be taken into account, the Fermi liquid behavior $\rho \propto T^2$ (at $T \ll E_0/10$) is not reproduced. In order to reproduce the T^2 -behavior, we need to take into account higher order terms of $O(1/N)^1$ as shown in ref. 14. However, the higher order correction is known not to appreciably affect the temperature dependence of ρ at $T > T_0$.¹⁵⁾ In Fig. 18(b), the T -dependences of n_f , n_c , and $n = n_c + n_f$, and ε_f are also displayed. The numerical calculation is performed under the condition that n is fixed.

In Fig. 19, the T -dependence of the resistivity $\rho(T)$ in both the cases of with and without CEF splitting are shown. $E_0(0)$ with CEF splitting becomes smaller than that in the absence of CEF splitting. In the inset of Fig. 18(a) and 19, the T -dependence of $E_0(T)$ is shown. We find that $E_0(4 \times 10^{-4}D) \sim 0.01D$ in the case of $\Delta_1 = \Delta_2 = 0$. This value is consistent with $E_0(0)$ derived from the calculation at $T = 0$ in §3.

5. Pressure Effect on Resistivity

In this section, we discuss the effect of pressure on the double-peak structure in the T -dependence of $\rho(T)$. In heavy fermion compounds such as CeCu_2Si_2 ,⁵⁾ the double peaks merge into a single peak with increasing pressure. We discuss this problem on the basis of the present model (infinite- U $J=5/2$ generalized PAM under a tetragonal symmetry) in which the effect of pressure is parameterized as that of the hybridization V between conduction electrons and f-electrons. We adopt the following parameters; $D = 1$, $n \equiv n_c + n_f = 1.4$, $\varepsilon_f^{(0)} = -0.7D$, and we set the CEF parameters as $\Delta_1 = 0.02D$ and $\Delta_2 = 0.04D$ putting the case of CeCu_2Si_2 ²⁴⁾ in mind. We illustrate the results of the calculation for a series of hybridization parameters V in Fig. 20. For $V^2 = 8.71 \times 10^{-3}D^2 \sim 1.0 \times 10^{-2}D^2$, the resistivity exhibits a double-peak structure, for $V^2 \gtrsim 1.28 \times 10^{-2}D^2$ the double-peak structure fades away, and a single-peak structure is obtained. Namely, we find the double peaks of the resistivity merge into a single peak when V is increased gradually, which is consistent with experiments under various pressures.

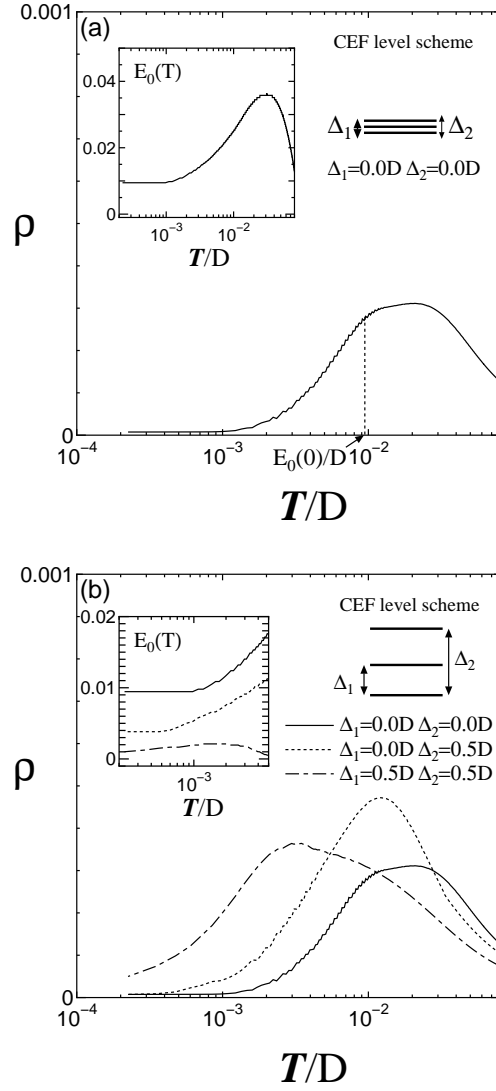


Fig. 19. (a) Temperature dependence of electrical resistivity $\rho(T)$ in case of $\Delta_1 = \Delta_2 = 0$, and (b) that for series of CEF-splitting schemes.

This result is summarized as follows. The Kondo temperature, which is related to the peak at lower temperatures, increases with increasing V (See Fig. 8(a)), so that one peak at a lower temperature shifts to a higher temperature monotonously with increasing V . On the other hand, in Fig. 20(b), another peak at a higher temperature shows only a slight shift to a lower temperature with increasing V . After that, the merged peak, which formed at $V^2 \gtrsim 1.28 \times 10^{-2}D^2$, shifts further to much higher temperatures with increasing V . This behavior describes the experimental results fairly well. For a hybridization $V^2 = 7.2 \times 10^{-3}D^2$ smaller than $V^2 = 8.1 \times 10^{-3}D^2$, the double-peak structure of the resistivity also becomes invisible. The parameter space in which $\rho(T)$ exhibits the double-peak structure is limited, and is dependent on the energy scale of Δ_1 and Δ_2 etc.

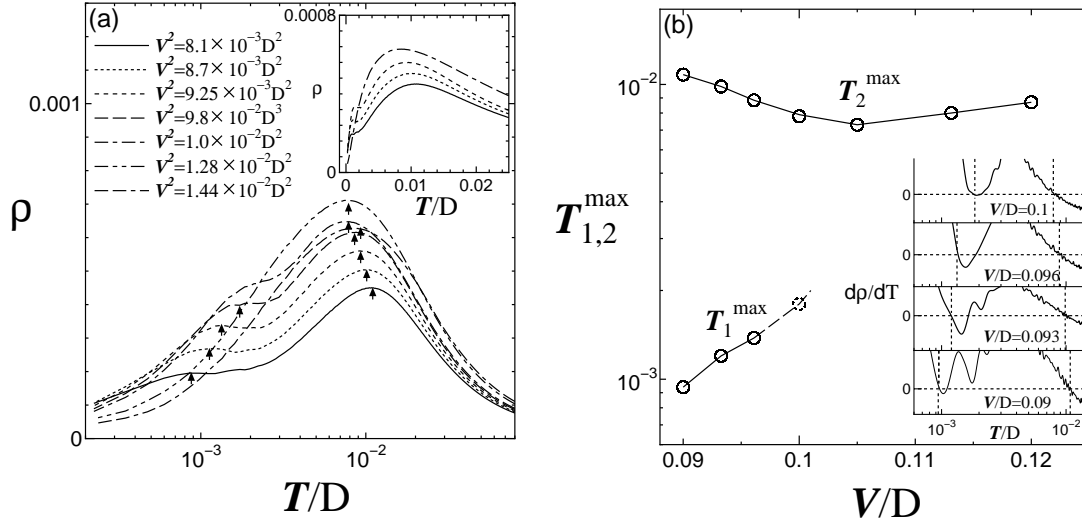


Fig. 20. (a) Temperature dependence of resistivity for a series of hybridization. Arrows indicate the temperatures T_1^{\max} and T_2^{\max} where $-\mathrm{d}\rho/\mathrm{d}T$ is zero. (b) $T_{1,2}^{\max}$ vs V in the case of the CEF splitting $\Delta_1 = 0.02D$, $\Delta_2 = 0.04D$.

6. Conclusions and Discussions

We have studied the behavior of the electrical resistivity $\rho(T)$ under pressure of Ce-based heavy fermion systems in the framework of a generalized periodic Anderson model (generalized PAM) in a manifold of $J = 5/2$ under a tetragonal configuration. We applied the $1/N$ -expansion method to the generalized PAM, and presented numerical results within an accuracy of $(1/N)^0$ for the calculation at finite temperatures as well as $T = 0$. Furthermore, by using the present extension of the $(1/N)$ -expansion method, we investigated the effect of pressure on the resistivity $\rho(T)$ by parameterizing the effect of the pressure as a variation of the hybridization between the conduction electrons and f-electrons. As a result, we reproduced the behavior that the double-peak structure in $\rho(T)$ is shown to merge into a single peak with increasing pressure, which is in good agreement with experiments for numerous heavy fermion compounds.

Here, we point out some remaining problems and perspectives. The present model may be too simplified for quantitative study in the sense that we have neglected the \mathbf{k} -dependence of the self-energy as well as the hybridization $V_{\mathbf{k}\Gamma\sigma}$. We may be able to discuss the \mathbf{k} -dependence of $V_{\mathbf{k}\Gamma\sigma}$ qualitatively by parameterizing the weight of the hybridization parameter V for each level Γ without setting V constant. On the other hand, the \mathbf{k} -dependence of the self-energy is treated by taking into account inter-site correlation which is observed in the higher order terms of $O(1/N)$. By studying the problem up to $O(1/N)^1$, we can discuss the inter-site correlation such as the RKKY interaction as detailed in ref. 25. Fundamental problems such as the competition between the RKKY interaction and the Kondo effect around quantum

critical point in the lattice system remain to be studied further.

Acknowledgement

We would like to thank Yoshiaki Ōno for valuable discussions and comments. This work is supported by a Grant-in-Aid for Scientific Research (No.16340103) and 21st Century COE Program (G18) from the Japan Society for the Promotion of Science.

Appendix A: Calculation of $G_f^i(\omega)_{(b)}$

In this appendix, we discuss the structure of $G_f^i(\omega)_{(b)}$ in detail. At $T = 0$, the analytical expression of eq. (3.29) is derived, while at a finite temperature $T \gtrsim E_0$ an additional term becomes important. From the diagrammatic representation in Fig. 11(b), we write $G_f^i(i\omega_n)_{(b)}$ as follows:

$$G_f^i(i\omega_n)_{(b)} = \frac{1}{N_L} \sum_{\Gamma\pm} \sum_{\sigma} \sum_{\mathbf{k}_\sigma} T \sum_{\omega'_n} T \sum_{\nu_n} |V_{\Gamma\sigma}|^2 G_{\mathbf{k}\sigma}(-i\omega'_n) B_i(i\nu_n) \times F_{i\Gamma}^2(i\omega_n + i\nu_n) B_i(i\omega_n + i\nu_n + i\omega'_n) / \langle \hat{Q} \rangle_\lambda. \quad (\text{A.1})$$

Here, we take the summation with respect to the Matsubara frequency,

$$G_f^i(i\omega_n)_{(b)} = -\frac{1}{N_L} \sum_{\Gamma\pm} \sum_{\sigma} \sum_{\mathbf{k}_\sigma} |V_{\Gamma\sigma}|^2 \int d\varepsilon f(\varepsilon) \left[\frac{-1}{\pi} \text{Im} G_{\mathbf{k}\sigma}(-\varepsilon + i0_+) \right] \times \frac{1}{2\pi i} \int_C d\varepsilon' n(\varepsilon') B_i(\varepsilon') F_{i\Gamma}^2(i\omega_n + \varepsilon') B_i(i\omega_n + \varepsilon + \varepsilon') / \langle \hat{Q}_i \rangle_\lambda, \quad (\text{A.2})$$

where $n(\varepsilon)$ is the Bose distribution function. Here, we also use the notation: $\bar{B}(\omega) = B_i(\omega + \lambda_i + \varepsilon_f)$ and $\langle \hat{Q}_i \rangle_\lambda = e^{-\beta(\lambda_i + \varepsilon_f - E_0)} \langle \hat{Q} \rangle$. Then, the above equation can be rewritten as

$$\begin{aligned} G_f^i(i\omega_n)_{(b)} &= -\frac{1}{N_L} \sum_{\Gamma\pm} \sum_{\sigma} \sum_{\mathbf{k}_\sigma} |V_{\Gamma\sigma}|^2 \int d\varepsilon f(\varepsilon) \left[\frac{-1}{\pi} \text{Im} G_{\mathbf{k}\sigma}(-\varepsilon + i0_+) \right] \\ &\quad \times \frac{1}{2\pi i} \int_C d\varepsilon' e^{-\beta(E_0 + \varepsilon')} \bar{B}(\varepsilon') F_{i\Gamma}^2(i\omega_n + \varepsilon') \bar{B}(i\omega_n + \varepsilon + \varepsilon') / \langle \hat{Q} \rangle, \\ &= -\frac{1}{N_L} \sum_{\Gamma\pm} \sum_{\sigma} \sum_{\mathbf{k}_\sigma} |V_{\Gamma\sigma}|^2 \int d\varepsilon f(\varepsilon) \left[\frac{-1}{\pi} \text{Im} G_{\mathbf{k}\sigma}(-\varepsilon + i0_+) \right] \\ &\quad \times \frac{1}{2\pi i} \int_C d\varepsilon' e^{-\beta(E_0 + \varepsilon')} \bar{B}(\varepsilon') F_{i\Gamma}^2(i\omega_n + \varepsilon') \bar{B}(i\omega_n + \varepsilon + \varepsilon') / \langle \hat{Q} \rangle, \\ &= \frac{1}{N_L} \sum_{\Gamma\pm} \sum_{\sigma} \sum_{\mathbf{k}_\sigma} |V_{\Gamma\sigma}|^2 \int d\varepsilon f(\varepsilon) \left[\frac{-1}{\pi} \text{Im} G_{\mathbf{k}\sigma}(-\varepsilon + i0_+) \right] / \langle \hat{Q} \rangle \\ &\quad \times \left[\int d\varepsilon' e^{-\beta(E_0 + \varepsilon')} \left[\frac{-1}{\pi} \text{Im} \bar{B}(\varepsilon' + i0_+) \right] \bar{B}(i\omega_n + \varepsilon + \varepsilon') \frac{1}{(i\omega_n + \varepsilon' - E_{i\Gamma} + \varepsilon_f)^2} \right. \\ &\quad \left. + \int d\varepsilon' e^{-\beta(E_0 - \varepsilon + \varepsilon')} \left[\frac{-1}{\pi} \text{Im} \bar{B}(\varepsilon' + i0_+) \right] \bar{B}(-i\omega_n - \varepsilon + \varepsilon') \frac{-1}{(\varepsilon' - \varepsilon - E_{i\Gamma} + \varepsilon_f)^2} \right. \\ &\quad \left. + \frac{d}{d\varepsilon'} \left[e^{-\beta(E_0 + \varepsilon')} \bar{B}(\varepsilon') \bar{B}(\varepsilon + \varepsilon' + i\omega_n) \right] \Big|_{\varepsilon' = -i\omega_n + E_{i\Gamma} - \varepsilon_f} \right]. \quad (\text{A.3}) \end{aligned}$$

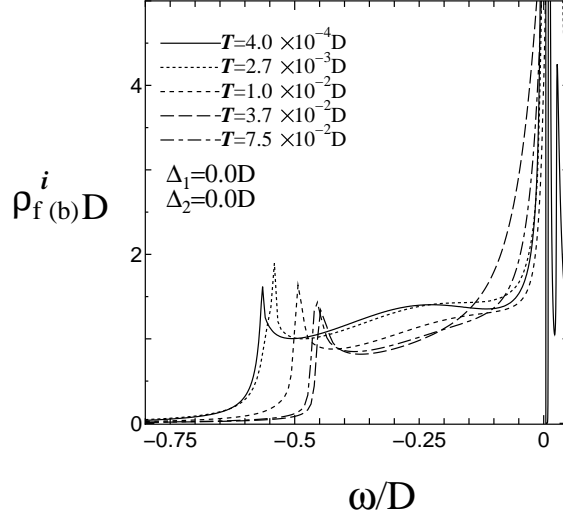


Fig. 21. $\rho_f^i(\omega)_{(b)}$ vs ω for a series of temperatures.

After performing the analytic continuation $i\omega_n \rightarrow \omega_+ \equiv \omega + i0_+$, and changing the variable $\varepsilon \rightarrow -\varepsilon$ in the second term, we obtain eq. (3.29). At $T = 0$, the third term, which is the contribution from the double pole of the pseudo-fermion, vanishes because of a factor $\exp(-\beta E_0)$.

At a finite temperature ($T \gtrsim E_0$), however, the third term in eq. (A.3) is non-vanishing. The contribution from $G_f^i(\omega)_{(b)}$ in Fig. 11(b), consists of both the pole of the slave-boson, $G_f^{i(bp)}(\omega)_{(b)}$, and the double poles of the pseudo-fermion, $G_f^{i(dp)}(\omega)_{(b)}$. Here, we define $\rho_f^i(\omega)_{(b)} = -1/\pi \text{Im} G_f^i(\omega)_{(b)}$, $\rho_f^{i(bp)}(\omega)_{(b)} = -1/\pi \text{Im} G_f^{i(bp)}(\omega)_{(b)}$, and $\rho_f^{i(dp)}(\omega)_{(b)} = -1/\pi \text{Im} G_f^{i(dp)}(\omega)_{(b)}$. Then,

$$\rho_f^i(\omega)_{(b)} = \rho_f^{i(bp)}(\omega)_{(b)} + \rho_f^{i(dp)}(\omega)_{(b)}, \quad (\text{A.4})$$

where

$$\begin{aligned} \rho_f^{i(bp)}(\omega)_{(b)} &= \sum_{\Gamma_{\pm}} \sum_{\sigma} |V_{\Gamma\sigma}|^2 \int d\varepsilon f(\varepsilon) \int d\varepsilon' e^{-\beta(E_0+\varepsilon')} \frac{-1}{\pi} \text{Im} \bar{B}(\varepsilon' + i0_+) / \langle \hat{Q} \rangle \\ &\times \left[\rho_{\sigma}(-\varepsilon) \cdot \frac{-1}{\pi} \text{Im} \bar{B}(\omega + \varepsilon + \varepsilon' + i0_+) \cdot \frac{1}{(\omega + \varepsilon' - E_{i\Gamma} + \varepsilon_f)^2} \right. \\ &\left. + \rho_{\sigma}(\varepsilon) \cdot \frac{-1}{\pi} \text{Im} \bar{B}(-\omega + \varepsilon + \varepsilon' + i0_+) \cdot \frac{1}{(\varepsilon + \varepsilon' - E_{i\Gamma} + \varepsilon_f)^2} \right], \quad (\text{A.5}) \end{aligned}$$

and

$$\begin{aligned} \rho_f^{i(dp)}(\omega)_{(b)} &= \sum_{\Gamma_{\pm}} \sum_{\sigma} |V_{\Gamma\sigma}|^2 \int d\varepsilon f(\varepsilon) \rho_{\sigma}(-\varepsilon) \cdot \left(\frac{-1}{\pi} \right) \cdot e^{-\beta(E_0+E_{i\Gamma}-\varepsilon_f)} / \langle \hat{Q} \rangle \\ &\times \left[-\frac{1}{T} \text{Im} \bar{B}(-\omega + E_{i\Gamma} - \varepsilon_f + i0_+) \bar{B}(\varepsilon + E_{i\Gamma} - \varepsilon_f) \right. \\ &\left. + \bar{B}(\varepsilon + E_{i\Gamma} - \varepsilon_f) \text{Im} \frac{d\bar{B}(\varepsilon' + i0_+)}{d\varepsilon'} \Big|_{\varepsilon' = -\omega + E_{i\Gamma} - \varepsilon_f} \right] \end{aligned}$$

$$+ \text{Im} \bar{B}(-\omega + E_{i\Gamma} - \varepsilon_f + i0_+) \frac{d\bar{B}(\varepsilon')}{d\varepsilon'} \Big|_{\varepsilon'=\varepsilon+E_{i\Gamma}-\varepsilon_f} \Big]. \quad (\text{A.6})$$

In Fig. 21, we show the temperature dependence of $\rho_f^i(\omega)_{(b)}$ as calculated numerically.

Appendix B: Kondo temperature in impurity case

In this appendix, we derive the relation between the Kondo temperature and the CEF-splitting in the impurity Anderson model, eq. (3.36). E_0 is defined as the binding energy of the slave-boson. At $T = 0$, E_0 corresponds to the Kondo temperature T_K defined in an impurity version of the Anderson model. In the impurity problem, the conduction electron is not renormalized, so we can put $E_0 \rightarrow T_K$, $\alpha_{\mathbf{k}\sigma}^j \rightarrow \varepsilon_{\mathbf{k}\sigma}$ and $A_{\mathbf{k}}^j \rightarrow 1$, in eq. (3.12):

$$\begin{aligned} T_K - \varepsilon_f &= \frac{1}{N_L} \sum_{\Gamma_{\pm}} \sum_{\sigma} \sum_{\mathbf{k}_{\sigma}} \frac{f(\varepsilon_{\mathbf{k}\sigma}) |V_{\Gamma\sigma}|^2}{T_K + E_{i\Gamma} - \varepsilon_f - \varepsilon_{\mathbf{k}\sigma}}, \\ &= \frac{V^2}{N_L} \sum_{\sigma} \sum_{\mathbf{k}_{\sigma}} \frac{f(\varepsilon_{\mathbf{k}\sigma})}{T_K - \varepsilon_{\mathbf{k}\sigma}} + \frac{V^2}{N_L} \sum_{\sigma} \sum_{\mathbf{k}_{\sigma}} \frac{f(\varepsilon_{\mathbf{k}\sigma})}{T_K + \Delta_1 - \varepsilon_{\mathbf{k}\sigma}}, \\ &\quad + \frac{V^2}{N_L} \sum_{\sigma} \sum_{\mathbf{k}_{\sigma}} \frac{f(\varepsilon_{\mathbf{k}\sigma})}{T_K + \Delta_2 - \varepsilon_{\mathbf{k}\sigma}}, \end{aligned} \quad (\text{B.1})$$

where we have used the following approximation: $\sum_{\pm} |V_{\Gamma\sigma}|^2 = \sum_{\pm} |V_{\Gamma\bar{\sigma}}|^2 = V^2$, where \sum_{\pm} means the summation over the Kramers doublets. Here, we assume $T_K \ll \Delta_1 \sim \Delta_2 \ll |\varepsilon_f| < |D|$, which is a reasonable assumption in an actual system, and $(1/N_L) \sum_{\mathbf{k}}$ is replaced by the integral $\rho_0 \int_{-D}^D d\varepsilon$, ρ_0 being the DOS of the conduction electron per spin at Fermi level. Then, eq. (B.1) is reduced to

$$\begin{aligned} -\varepsilon_f &\simeq 2V^2 \rho_0 \int_{-D}^D d\varepsilon f(\varepsilon) \frac{1}{T_K - \varepsilon} \\ &\quad + 2V^2 \rho_0 \int_{-D}^D d\varepsilon f(\varepsilon) \frac{1}{\Delta_1 - \varepsilon} + 2V^2 \rho_0 \int_{-D}^D d\varepsilon f(\varepsilon) \frac{1}{\Delta_2 - \varepsilon}. \end{aligned} \quad (\text{B.2})$$

On the basis of this equation at $T = 0$, the Kondo temperature T_K is evaluated as follows: ε -integration in (B.2) is performed explicitly, leading to

$$\begin{aligned} \varepsilon_f &= 2V^2 \rho_0 \log \left| \frac{D - T_K}{T_K} \right| + 2V^2 \rho_0 \log \left| \frac{D - \Delta_1}{\Delta_1} \right| + 2V^2 \rho_0 \log \left| \frac{D - \Delta_2}{\Delta_2} \right|, \\ &\simeq 2V^2 \rho_0 \log \left| \frac{D}{T_K} \right| + 2V^2 \rho_0 \log \left| \frac{D}{\Delta_1} \right| + 2V^2 \rho_0 \log \left| \frac{D}{\Delta_2} \right|. \end{aligned} \quad (\text{B.3})$$

Then, it is easy to find a solution for T_K as

$$T_K = D \cdot \left(\frac{D}{\Delta_1} \right) \cdot \left(\frac{D}{\Delta_2} \right) \exp \left(-\frac{|\varepsilon_f|}{2\rho_0 V^2} \right). \quad (\text{B.4})$$

Similarly, we can calculate the Kondo temperature $T_K^{(0)}$ in the absence of CEF splitting. By putting $\Delta_1 = \Delta_2 = 0$ in eq. (B.1), we obtain

$$T_K^{(0)} - \varepsilon_f = 3 \frac{V^2}{N_L} \sum_{\sigma} \sum_{\mathbf{k}_{\sigma}} \frac{f(\varepsilon_{\mathbf{k}\sigma})}{T_K^{(0)} - \varepsilon_{\mathbf{k}\sigma}}. \quad (\text{B.5})$$

Hence,

$$T_K^{(0)} = D \exp\left(-\frac{|\varepsilon_f|}{6\rho_0 V^2}\right). \quad (\text{B.6})$$

From the relations between T_K and $T_K^{(0)}$, we can derive equation (3.36):

$$\left[T_K^{(0)}\right]^3 = \Delta_1 \cdot \Delta_2 \cdot T_K. \quad (\text{B.7})$$

In the leading order, the result with use of $1/N$ -expansion method in case of the impurity problem, is consistent with the previous impurity study.^{20,21)}

Appendix C: The algorithm for self-consistent $1/N$ -expansion

In this appendix, we explain the algorithm of self-consistent $1/N$ -expansion over the entire temperature range. The whole procedure is summarized as follows:

1) Self-energy of conduction electron

First, we choose the self-energy $\Sigma_{\mathbf{k}\sigma}(\omega)$ of the conduction electron as a trial function. If we start from the low-temperature region, we can choose $\Sigma_{\mathbf{k}\sigma}(\omega)$ derived from low-temperature approximation, eq. (3.6), i.e.,

$$\Sigma_{\mathbf{k}\sigma}(\omega) = \sum_{\Gamma\pm} \frac{a|V_{\mathbf{k}\Gamma\sigma}|^2}{\omega - E_0 - E_{i\Gamma} + \varepsilon_f}, \quad (\text{C.1})$$

where E_0 and a is obtained by the coupled self-consistent equations at $T = 0$, eqs. (3.12) \sim (3.14). We restrict the range of the energy, from $-\omega_{\max}$ to ω_{\max} . In an actual numerical calculation, ω is defined as a discrete value ω_j ($j = -j_{\max}, -j_{\max} + 1, \dots, j_{\max} - 1, j_{\max}$), where j_{\max} is an integer of maximum cut number of the energy. For example, we define ω_j as follows:

$$\omega_j = \frac{j^2}{j_{\max}^2} \omega_{\max}. \quad (\text{C.2})$$

We use $\omega_{\max} = 2D$ and $j_{\max} = 700$ in the present paper.

2) Green function of the conduction electron

The Green function of the conduction electron is obtained from the above self-energy as

$$G_{\mathbf{k}\sigma}(\omega) = \frac{1}{\omega - \varepsilon_{\mathbf{k}\sigma} + \mu - \Sigma_{\mathbf{k}\sigma}(\omega)}, \quad (\text{C.3})$$

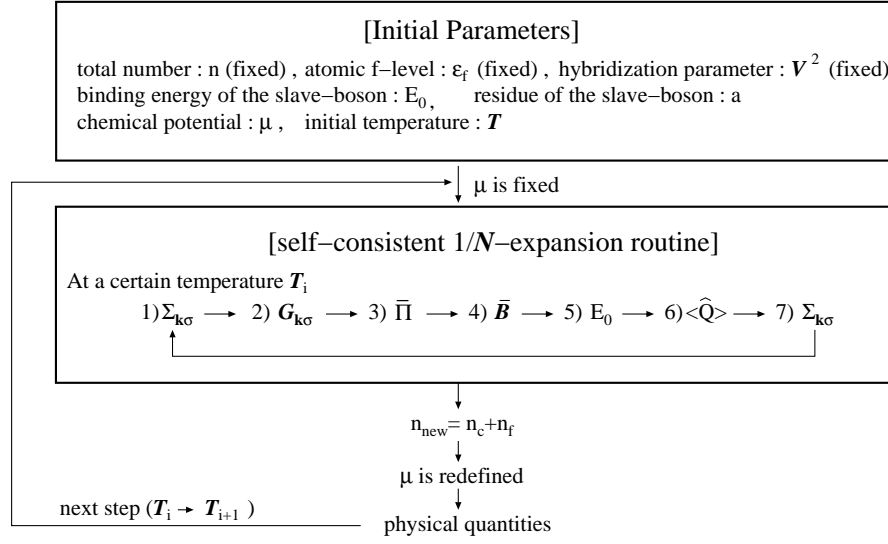
where μ is the chemical potential. Then, $(\frac{1}{N_L}) \sum_{\mathbf{k}\sigma} G_{\mathbf{k}\sigma}(\omega)$ is performed as follows,

$$\begin{aligned} \frac{1}{N_L} \sum_{\mathbf{k}\sigma} G_{\mathbf{k}\sigma}(\omega) &= \rho_0 \int_{-D}^D d\varepsilon \frac{1}{\omega - \varepsilon + \mu - \Sigma_{\mathbf{k}\sigma}(\omega)}, \\ &= \frac{1}{2D} \log \frac{\omega + D + \mu - \Sigma_{\mathbf{k}\sigma}(\omega)}{\omega - D + \mu - \Sigma_{\mathbf{k}\sigma}(\omega)}, \end{aligned} \quad (\text{C.4})$$

where $\rho_0 \equiv 1/2D$ as in eq. (3.16), and $\mu \equiv 0$ in our numerical calculation.

3) Self-energy of slave-boson

The imaginary part of the self-energy $\text{Im}\bar{\Pi}(\omega)$, eq. (2.51), of the slave-boson is calculated

Fig. 22. An example algorithm for self-consistent $1/N$ -expansion.

by using $G_{\mathbf{k}\sigma}$, eq. (C.3), as

$$\text{Im}\bar{\Pi}(\omega) = \sum_{\Gamma\pm} \sum_{\sigma} \sum_{\mathbf{k}\sigma} \frac{|V_{\mathbf{k}\Gamma\sigma}|^2}{N_L} f(-\omega + E_{i\Gamma} - \varepsilon_f) \text{Im}G_{\mathbf{k}\sigma}(-\omega + E_{i\Gamma} - \varepsilon_f). \quad (\text{C.5})$$

$\text{Re}\bar{\Pi}(\omega)$ is calculated by the Kramers-Krönig relation. Hence, we can obtain $\bar{\Pi}(\omega) = \text{Re}\bar{\Pi}(\omega) + i \cdot \text{Im}\bar{\Pi}(\omega)$

4) Green function of slave-boson

The Green function $\bar{B}(\omega)$ of the slave-boson is given as

$$\bar{B}(\omega) = \frac{1}{\omega + \varepsilon_f - \bar{\Pi}(\omega)}. \quad (\text{C.6})$$

5) Determination of $E_0(T)$

The binding energy of the slave-boson $E_0(T)$ defined as the real part of the pole of $\bar{B}(\omega)$, eq. (C.6). However, in actual calculation, we approximate it as the value which satisfies the following equation:

$$\varepsilon_f - E_0(T) = \text{Re}\bar{\Pi}(-E_0(T)). \quad (\text{C.7})$$

This equation is an approximation of eq. (2.54).

6) Calculation of $\langle \hat{Q}_i \rangle_\lambda$

We have defined $\langle \hat{Q}_i \rangle_\lambda = e^{-\beta(\lambda_i + \varepsilon_f - E_0(T))} \langle \hat{Q} \rangle$, where $E_0(T)$ is obtained by procedure 5). We calculate $\langle \hat{Q} \rangle$ from eqs. (2.39), (2.48), and (2.49) by using the Green function of the conduction electron in procedure 2), the slave-boson in procedure 4), and the pseudo-fermion.

7) Self-energy of conduction electron

Finally, through the procedures 2) ~ 6), we can calculate $\Sigma_{\mathbf{k}\sigma}$ again by eq. (2.43) as

$$\text{Im}\Sigma_{\mathbf{k}\sigma}(\omega) = \sum_{\Gamma\pm} |V_{\mathbf{k}\Gamma\sigma}|^2 (1 + e^{\beta\omega}) e^{-\beta(E_0(T) + E_{i\Gamma} - \varepsilon_f)} \cdot \text{Im}\bar{B}(-\omega + E_{i\Gamma} - \varepsilon_f). \quad (\text{C.8})$$

$\text{Re}\Sigma_{\mathbf{k}\sigma}(\omega)$ is derived from the Kramers-Krönig relation. As a result, we can obtain the newly defined $\Sigma_{\mathbf{k}\sigma}(\omega) \equiv \text{Re}\Sigma_{\mathbf{k}\sigma}(\omega) + i \cdot \text{Im}\Sigma_{\mathbf{k}\sigma}(\omega)$.

This series of procedures, 1)~7), forms a self-consistent cycle. We show the concept chart of this cycle in Fig. 22. In our calculation, this procedure was performed with fixed n , the total number of electron per site. In order to check the self-consistency, we define the following amount,

$$\delta\text{Im}\bar{\Pi} = \frac{\sum_{j=-j_{\max}}^{j_{\max}} |\text{Im}\bar{\Pi}_{\text{new}}(\omega_j) - \text{Im}\bar{\Pi}_{\text{old}}(\omega_j)|}{2j_{\max} + 1}. \quad (\text{C.9})$$

$\text{Im}\bar{\Pi}_{\text{new}}(\omega)$ is a new $\text{Im}\bar{\Pi}(\omega)$ obtained from one cycle by using $\text{Im}\bar{\Pi}_{\text{old}}(\omega)$. This self-consistent cycle is repeated until $\delta\text{Im}\bar{\Pi}(\omega)$ becomes less than $10^{-4}D \sim 10^{-5}D$. By performing this procedure for each temperature, we can calculate the temperature dependence of physical quantities such as the electrical resistivity.

References

- 1) A. Sumiyama, Y. Oda, H. Nagano, Y. Ōnuki, K. Shibutani and T. Komatsubara: J. Phys. Soc. Jpn. **55** (1986) 1294.
- 2) Y. Ōnuki, Y. Furukawa and T. Komatsubara: J. Phys. Soc. Jpn. **53** (1984) 2734.
- 3) E. Vargoz, P. Link, D. Jaccard, T. Le Bihan and S. Heathman: Physica B **229** (1997) 225.
- 4) P. Link and D. Jaccard: Physica B **230** (1997) 31.
- 5) A. T. Holes, D. Jaccard and K. Miyake: Phys. Rev. B **69** (2004) 024508.
- 6) D. Jaccard, H. Wilhelm, K. Alami-Yadri and E. Vargoz: Physica B **259-261** (1999) 1.
- 7) S. Maekawa, S. Takahashi S. Kashiba and M. Tachiki: J. Phys. Soc. Jpn. **54** (1985) 1955.
- 8) A. Nakamura, N. Kawakami and A. Okiji: J. Phys. Soc. Jpn. **56** (1987) 3667.
- 9) Y. Ōno, T. Matsuura and Y. Kuroda: Physica C **159** (1989) 878.
- 10) Y. Ōno, T. Matsuura and Y. Kuroda: J. Phys. Soc. Jpn. **60** (1991) 3475.
- 11) H. Kontani and K. Yamada: J. Phys. Soc. Jpn. **65** (1996) 172.
- 12) P. Coleman: Phys. Rev. B **29** (1984) 3035.
- 13) H. Kontani, M. Miyazawa and K. Yamada: J. Phys. Soc. Jpn. **66** (1997) 2252.
- 14) A. Tsuruta, A. Kobayashi, K. Deguchi, Y. Ōno, T. Matsuura and Y. Kuroda: J. Phys. Soc. Jpn. **68** (1999) 1067.
- 15) A. Tsuruta, A. Kobayashi, T. Matsuura and Y. Kuroda: J. Phys. Soc. Jpn. **69** (2000) 3342.
- 16) B. Jin and Y. Kuroda: J. Phys. Soc. Jpn. **57** (1988) 1687.
- 17) J. M. Luttinger: Phys. Rev. **119** (1960) 1153.
- 18) T. M. Rice and K. Ueda: Phys. Rev. B **34** (1986) 6420.
- 19) H. Shiba: J. Phys. Soc. Jpn. **55** (1986) 2765.
- 20) K. Yamada, K. Yosida and K. Hanzawa: Prog. Theor. Phys. **71** (1984) 450.
- 21) K. Hanzawa, K. Yamada and K. Yosida: J. Magn. Magn. Mater. **47 & 48** (1985) 357.
- 22) R. Kubo: J. Phys. Soc. Jpn. **12** (1957) 570.
- 23) A. A. Abrikosov, L. P. Gorkov and I. Ye. Dzyaloshinskii: *Quantum Field Theoretical Methods in Statistical Physics* (Pergamon Press, Oxford, 1965) 2nd ed., Sect. 19.
- 24) S. Horn, E. Holland-Moritz, M. Loewenhaupt, F. Steglich, H. Scheuer, A. Benoit, and J. Flouquet: Phys. Rev. B **23** (1981) 3171.
- 25) T. Kasuya: Prog. Theor. Phys. **16** (1956) 45.